TOPICAL REVIEW

Lattice methods for strongly interacting many-body systems

Joaquín E. Drut[1,2], **Amy N. Nicholson**[3]

[1] Theoretical Division, Los Alamos National Laboratory, Los Alamos, NM 87545-0001, USA
[2] Department of Physics and Astronomy, University of North Carolina, Chapel Hill, NC 27599-3255, USA
[3] Maryland Center for Fundamental Physics, Department of Physics, University of Maryland, College Park, MD 20742-4111, USA

E-mail: drut@email.unc.edu, amynn@umd.edu

Abstract.
Lattice field theory methods, usually associated with non-perturbative studies of quantum chromodynamics, are becoming increasingly common in the calculation of ground-state and thermal properties of strongly interacting non-relativistic few- and many-body systems, blurring the interfaces between condensed matter, atomic and low-energy nuclear physics. While some of these techniques have been in use in the area of condensed matter physics for a long time, others, such as hybrid Monte Carlo and improved effective actions, have only recently found their way across areas.

With this topical review, we aim to provide a modest overview and a status update on a few notable recent developments. For the sake of brevity we focus on zero-temperature, non-relativistic problems. After a short introduction, we lay out some general considerations and proceed to discuss sampling algorithms, observables, and systematic effects. We show selected results on ground- and excited-state properties of fermions in the limit of unitarity. Appendices include technical details on group theory and selected derivations.

Contents

1. Introduction

The term 'lattice methods' is commonly used to refer to a set of computational physics tools whose unifying idea consists in describing the spacetime continuum as a (generally hypercubic) mesh, of finite volume V and finite spacing b. Quantum fields are then defined on such a spacetime grid and the many-body problem thus becomes a problem with a finite number of degrees of freedom. As a matter of convenience, the corresponding partition function is typically represented in terms of Euclidean path integrals.

The fundamental reason for employing lattice methods to treat a given problem is that in many cases of interest the resulting path integral can be evaluated stochastically using computers, in a fashion that is both efficient and in principle exact. Indeed, assuming the problem is such that a proper probability measure can be defined, the stochastic calculation of the lattice path integral will suffer only from statistical uncertainties, which can be precisely quantified. Furthermore, errors associated with the use of finite volumes V and finite lattice spacings b, are also controlled and can be systematically removed by using larger V, smaller b, and/or improved actions. Thus, lattice methods, when applicable, surpass perturbative as well as mean-field approaches in the quest for the reliable quantitative characterization of quantum many-body systems. This is true in particular if those systems are close to a phase transition, or if they are in any way strongly correlated, by which we mean that the low-energy excitations (and thus the long-distance properties) of the system are dramatically different from those of a system with the same degrees of freedom but no interactions.

On the other hand, lattice methods are not the only available numerical approaches for strongly coupled many-body physics. Other potentially exact techniques such as Green's function Monte Carlo (GFMC) [1, 2, 3], Coupled Cluster (CC) [4, 5] and No-Core Shell Model (NCSM) [6] are in the mainstream, especially in modern studies of nuclear structure (see e.g. [7, 8, 9, 10, 11, 12, 13, 14, 15, 16, 17, 18, 19, 20]). Still, it should be pointed out that GFMC involves the uncontrolled fixed-node approximation, and while this has not prevented practitioners from obtaining remarkably accurate results, it is regarded by many as intellectually somewhat dissatisfying. Uncontrolled approximations aside, none of these methods scales with the size of the problem as favorably as current lattice approaches. In addition, lattice methods have robust technical foundations and benefit from a continuous stream of attention from the Lattice QCD community.

Apart from explaining the motivations for using and developing lattice methods, and setting the broad context, the purpose of this Introduction is to establish the scope for the rest of the article. We have decided to focus our attention on methods for non-relativistic systems, more specifically for ground-state calculations. There are several excellent books and reviews on relativistic systems, particularly on those with gauge degrees of freedom (see e.g. Refs. [21, 22, 23]), and the topic of finite temperature merits a separate article by itself (see e.g. Refs. [24, 25]). We shall also avoid the all-important issues of time-dependent response functions and their analytic continuation to real time, which are topics that deserve their own review articles (see e.g. [26, 27]).

The motivation for the investigation of lattice methods specifically for non-relativistic systems is at least twofold. On one hand, the behavior of the vast majority of atomic and condensed-matter systems is governed by electronic Hamiltonians in

which relativistic effects enter only as a small correction. The symmetry group is thus not given by the Poincaré set of Lorentz boosts and spacetime translations, but rather by rotations and Galilei transformations, or their discrete counterparts when a physical lattice is present. It should be stressed, however, that the richness of low-energy condensed-matter physics allows for an immense array of Hamiltonians whose characterization defies the above simple-minded binary approach. At this point in time perhaps the paradigm of this situation is given by graphene, whose low-energy dynamics is controlled by a (relativistic-like) linear dispersion relation plus a (certainly non-relativistic) Coulomb interaction. While a few groups are currently using lattice field theory methods to elucidate the effects of strong coupling in graphene (see e.g. Refs. [28, 29, 30, 31, 32, 33, 34]), we shall not discuss this system beyond this point.

The other main motivation comes from low-energy nuclear physics, where the description is predominantly given by non-relativistic actions, as the mass of the nucleons ($\sim$ 1 GeV) is much larger than the mass of the low-energy excitations ($m_\pi \simeq 0.1$ GeV), which are pseudo-Goldstone bosons associated with the spontaneous breaking of an approximate chiral symmetry (see Ref. [35]). Lattice calculations of nuclei are still in their infancy, but are currently being aggressively pursued by the Bonn-Raleigh group [36, 37, 38], having performed calculations of the lightest nuclei up to ^{12}C [39, 40], including a first study of the Hoyle state [41, 42]. Although they are beyond the scope of this review, the efforts of the NPLQCD collaboration [43, 44], dedicated to ab initio nuclear physics starting from Lattice QCD, should not be overlooked in this context.

Finally, it should be pointed out that there are dynamic synergistic activities among the various areas mentioned above. Indeed, with the advent of ultracold atom experiments in the last few years (see Ref. [45, 46, 47] for reviews of the current experimental and theoretical situation), the nuclear- and atomic-physics communities are working in close collaboration with each other. This applies in particular to the study of ultracold Fermi gases close to a Feshbach resonance. The latter are effectively spin-1/2 systems whose interaction can be tuned to vanishing range r_0 and large s-wave scattering length a_S. This seemingly "unnatural" situation is actually very much relevant for nuclear structure in general and neutron matter in particular, where the ranges are short ($r_0 \simeq 2.7$ fm) and the scattering lengths are large ($a_S \simeq -18$ fm). The stark difference between the nuclear scales ($\sim$ fm) and the atomic ones ($\sim$Å) testifies for the property of *universality* of the underlying dynamics [48, 49, 50].

Universality is particularly evident in the case of the so-called unitary Fermi gas, which is defined as the limit $0 \leftarrow k_F r_0 \ll 1 \ll k_F a_S \to \infty$, where $k_F = (3\pi^2 n)^{1/3}$ is the Fermi wave number and n is the density. By definition, the unitary limit has no intrinsic scales other than its density n and temperature T. As a consequence, every dimensionful thermodynamic quantity must come as a power of k_F, or equivalently the Fermi energy $\varepsilon_F = \hbar^2 k_F^2/(2M)$ (where M is the mass of the fermions) times a universal function of T/ε_F (or equivalently $\beta\mu$, where $\beta^{-1} = k_B T$ and μ is the chemical potential). In particular, one of the most sought-after universal functions corresponds to the energy, which is typically denoted by ξ and often referred to as the Bertsch parameter.

For the same reasons, the unitary Fermi gas displays a number of dynamical symmetries and exact relationships. Indeed, as shown in Refs. [51, 52], the unitary limit respects a non-relativistic conformal symmetry (Schödinger algebra [53, 54]). This symmetry is directly related to an exact relation between the scaling dimensions of the primary operators of the non-relativistic conformal field theory (which is defined

in free space) and the spectrum of the system in a harmonic trap [55, 56, 57, 58].

Aside from those relations, valid in the limit of infinite scattering length, there are a set of exact universal relations, now widely known as the Tan relations [59, 60, 61, 62, 63, 64, 65, 66, 67] (see Ref. [68] for a recent review), that encode the physics at short distances and which are due to the short-range nature of the interaction. The latter property allows one to write down explicit relations in terms of the probability of finding two particles of unequal spin at short distances from each other; this probability is commonly referred to as the "contact". At unitarity, the contact constitutes another universal property of quantum many-body physics. The Tan relations are valid at all temperatures and couplings, and have also been generalized to spatial dimensions other than 3, as well as to bosonic and fermionic systems. The precise calculation of the contact in most of these cases is still an open problem as of this writing.

In this review we shall be only indirectly concerned with the physics of the unitary limit, mostly as a test case for the various methods. While this limit is easy to define and implement in few- and many-body calculations, it has remained challenging to arrive at precise numerical answers for various quantities such as the Bertsch parameter and the contact. This is true not only of analytic methods, most of which break down in one way or another when approaching unitarity, but also for purely numerical methods. For these reasons, this problem is currently one of the most important benchmarks for few- and many-body methods in atomic and nuclear physics.

The rest of the article is organized as follows: in Sec. 2 we discuss the general process of formulating the many-body problem on a lattice, and give a first glimpse into improvement procedures. In Sec. 3 we present a sample of the current algorithms on the market for generating field configurations to be used in the stochastic estimation of the path integral. Sec. 4 demonstrates some of the various observables which may be calculated on a given set of configurations, focusing on ground-state observables. Sec. 5 then discusses difficulties associated with the extraction of the ground-state, and provides some techniques for dealing with these problems. In Sec. 6 we consider the issue of systematic errors induced by the use of a finite set of lattice points. Finally, we present a small selection of results obtained using the methods outlined in this article in Sec. 7, followed by our Conclusions (Sec. 8). An appendix reviewing the concept of group theory on the lattice is also provided (App. 9).

2. General considerations

The main objective of this section is to develop the connection between textbook many-body formalism and the expressions commonly used in actual numerical calculations. Ultimately, the goal is to develop expressions that allow us to evaluate expectation values of quantum operators $\hat{O}$ in a stochastic fashion, such that, up to systematic effects (finite volume, finite lattice spacing, etc.), the exact result is given (schematically) by

$$\langle \hat{O} \rangle = \frac{1}{\mathcal{Z}} \sum_n \mathcal{P}_n O_n \tag{1}$$

where $\mathcal{Z} = \sum_n \mathcal{P}_n$ and $\mathcal{P}_n$ is a positive semi-definite probability measure whose form depends on the problem under consideration, though generally not on the observable $\hat{O}$. Here, n parametrizes the values of a set of auxiliary variables (typically fields that live in spacetime), and it is the sum over their (usually unfathomably large) domain that is performed using Monte Carlo methods. If one succeeds in doing so, the result is then given by

$$\langle \hat{O} \rangle \simeq \frac{1}{N_s} \sum_{n=1}^{N_s} O_n, \tag{2}$$

where N_s is the number of samples of the auxiliary variables, distributed according to $\mathcal{P}_n$, and the uncertainty in the approximation is of order $1/\sqrt{N_s}$ if the samples are uncorrelated and assuming the central limit theorem holds. The quantity O_n is the expectation value of $\hat{O}$ in the n-th auxiliary configuration.

Naturally, limitations arise in the kinds of problems that can be treated in this fashion, as it is not always possible (or at least not easy) to define a positive semi-definite $\mathcal{P}_n$. This is of course the well-known sign-problem that appears in many problems of interest. We shall return to these and related issues below, and restrict ourselves to cases where the sign problem is absent.

Rather than focusing on specific observables, it is often more useful to attempt to re-write the partition function $\mathcal{Z}$ as a sum of positive terms, as mentioned above. As we shall see, in many cases this sets a natural framework for the calculation of any observable.

2.1. Starting point: the partition function & the transfer matrix

As mentioned in the Introduction, we shall focus on ground-state approaches for non-relativistic systems. However, it is convenient to set up the formalism by considering the general case of non-zero temperature T. In the grand-canonical ensemble, the thermodynamic properties of a quantum many-body system are fully specified by the partition function

$$\mathcal{Z} = e^{-\beta\Omega} = \mathrm{Tr}\, e^{-\beta(\hat{H}-\mu\hat{N})}, \tag{3}$$

where Ω is the grand thermodynamic potential, the trace is over all multi-particle states, i.e. over the Fock space, and $\beta = (k_B T)^{-1}$. In second-quantization language the Hamiltonian is given, in general, by

$$\hat{H} = h^{(1)}_{\alpha\beta}\hat{a}^\dagger_\alpha\hat{a}_\beta + h^{(2)}_{\alpha\beta\gamma\delta}\hat{a}^\dagger_\alpha\hat{a}^\dagger_\beta\hat{a}_\gamma\hat{a}_\delta + h^{(3)}_{\alpha\beta\gamma\delta\mu\nu}\hat{a}^\dagger_\alpha\hat{a}^\dagger_\beta\hat{a}^\dagger_\gamma\hat{a}_\delta\hat{a}_\mu\hat{a}_\nu + \cdots, \tag{4}$$

and the particle number is simply

$$\hat{N} = \hat{a}^\dagger_\alpha\hat{a}_\alpha, \tag{5}$$

where sums over repeated indices are implied, and $\hat{a}^\dagger_\alpha$ ($\hat{a}_\alpha$) is the creation (annihilation) operator of particles in state α, for a given choice of single-particle states $|\alpha\rangle$.

In Eq. (4) we have written a rather general Hamiltonian including not only the conventional one- and two-body terms, but also three- and higher-body interactions. We take the point of view that the Hamiltonian in question is *effective*, in the sense that it describes the physics of the problem below a certain scale Λ, and all the processes above that scale are encoded in the so-called low-energy constants $h^{(j)}(\Lambda)$, and higher-body interactions [69, 70]. This is expected to be a practicable approach when there is a clear separation of scales in the system. While this is the philosophy of modern effective field theory (EFT), with few exceptions most Monte Carlo calculations include only two-body interactions. Such a simplified theory can be an accurate description of dilute atomic systems or neutron matter in the crust of neutron stars (where the range of the interaction is small compared to the inter-particle distance), but fails at higher densities as well as for nuclear structure calculations. Concerning the latter, we expect vigorous research in this direction in the coming years, as the application of lattice methods to nuclear physics (with nucleons and pions as the elementary degrees of freedom) is currently gathering significant momentum, as mentioned in the Introduction. In this review we shall focus on two-body interactions only, but we shall comment on the difficulties of implementing higher-body interactions below.

Following the usual route (see e.g. Refs. [71, 72]), one may introduce a coherent-state representation and go on to the language of fields (with Grassmann fields for fermions and complex fields for bosons), such that the partition function of the problem at hand becomes

$$\mathcal{Z} = \int \mathcal{D}\psi^\dagger \mathcal{D}\psi \; e^{-S[\psi^\dagger,\psi]}. \tag{6}$$

From this point on we shall focus on the fermionic case, such that ψ denotes in general a multicomponent Grassmann field ψ_α, where $\alpha = 1, \ldots, N_f$, and N_f is the number of fermion flavors present in the problem. The Euclidean action is given by

$$S[\psi^\dagger,\psi] = \int d\tau d^3x \left(\psi^\dagger_\alpha(\partial_\tau - \mu)\psi_\alpha + \mathcal{H}[\psi^\dagger,\psi]\right), \tag{7}$$

and the Hamiltonian density reads

$$\mathcal{H} = \psi^\dagger_\alpha \hat{H}_0 \psi_\alpha + \ldots, \tag{8}$$

where we have implicitly summed over the flavors α, and the interaction terms are in the ellipsis. Here, $\hat{H}_0$ is a differential operator corresponding to the coordinate space representation of $h^{(1)}_{\alpha\beta}$ in Eq. (4). The full Hamiltonian is of course given by

$$H = \int d^3x \; \mathcal{H}[\psi^\dagger,\psi]. \tag{9}$$

The fields are defined in all of spacetime, where it should be kept in mind that at finite temperature the time direction is compact, extending from $\tau = 0$ to $\tau = \beta$. Fermionic (bosonic) fields obey anti-periodic (periodic) boundary conditions at the endpoints of the temporal direction. This is the starting point for the formulation of the problem in terms of lattice field theory.

We have thus started from a physical perspective by considering the grand-canonical partition function, and moved on to the language of fields, which provides the connection with modern methods often seen in Lattice QCD. In spite of the (sometimes considerable) technical differences, all of the methods we shall discuss here, and the

vast majority of the ground-state methods currently in use, actually share a common essential aspect. Indeed, they all rely on the so-called "power" method to extract from a given matrix (here the transfer matrix, defined below) the largest eigenvalue and eigenvector (here the ground state) (see e.g. Ref. [73]). The idea of starting with the finite-temperature formalism and taking the zero-temperature $\beta \to \infty$ limit is indeed nothing other than taking powers of the transfer matrix

$$\mathcal{T}_t = e^{-t\hat{H}}, \tag{10}$$

as a filtering process to systematically project out the excited states, assuming that one starts with a trial state that has a non-zero (and ideally very large) projection on the true ground state. In the language of fields this amounts to the determination of the mass gap (or in general, spectral properties) of the fermion propagator by selecting an optimal source.

We shall return to this idea below. In order to appreciate the connection between the various methods, which typically come from different areas, it is important to be able to jump between the "fields" and "transfer-matrix" languages. We anticipate that for many readers this connection will seem trivial. However, it is our experience that this is not the norm.

2.2. Putting the problem on the lattice

The next step is to discretize spacetime into $N_x^3 \times N_\tau$ points, and define fields on such a lattice. Throughout this review we shall consider a hypercubic lattice with lattice spacings $b_s, b_\tau \equiv \frac{b_s^2}{M}$ corresponding to the spatial and temporal directions, respectively, as that is by far the most common choice. We denote with $\psi_{\mathbf{n},\tau}$ the Grassmann field defined on all the space-time points $\mathbf{n}, \tau$, and $\psi^\dagger_{\mathbf{n},\tau}$ denotes its hermitian conjugate. The lattice Hamiltonian is then

$$H = \sum_{\mathbf{n},\mathbf{m}} \psi^\dagger_{\mathbf{n}} \left[H_0\right]_{\mathbf{n},\mathbf{m}} \psi_{\mathbf{m}} + \dots, \tag{11}$$

where $\mathbf{n}, \mathbf{m}$ are points on the spatial lattice, and $\left[H_0\right]_{\mathbf{n},\mathbf{m}}$ is a particular choice of a discrete representation for the continuum Hamiltonian $\hat{H}_0$. In most cases relevant for this review, the Hamiltonian will be time-independent. We have again omitted the interaction terms, which we turn to below.

In the absence of interactions, the dispersion relation for a non-relativistic system is of course $E = p^2/(2M)$, where M is the fermion mass. The choice of a discretized derivative, to represent the momentum operator in coordinate space, determines the form of the Hamiltonian of the non-interacting system on the lattice. The various choices differ in their approach to the continuum limit, i.e. in their behavior at high energies. For the Laplacian operator, the simplest choice is given by the second difference formula

$$\Delta f_{\mathbf{j}} \equiv \sum_{k=1,2,3} \frac{1}{b_s^2} \left[f_{\mathbf{j}+\mathbf{e}_k} + f_{\mathbf{j}-\mathbf{e}_k} - 2 f_{\mathbf{j}} \right], \tag{12}$$

where $\mathbf{e}_k$ is the unit vector in the k-th direction. This yields the correct behavior at low energies, as it gives the following kinetic-energy spectrum

$$E(\mathbf{p}) = \frac{2\hbar}{M b_s^2} \sum_{k=1,2,3} \sin^2\left(\frac{q_k}{2}\right), \tag{13}$$

where $\mathbf{p} = \hbar\mathbf{q}/b_s$, and $q_k = \frac{2\pi n_k}{N_x}$ takes on discrete values as $n_k = -N_x/2, \ldots, N_x/2$. Clearly, the above reproduces $E(\mathbf{p}) \simeq \frac{\mathbf{p}^2}{2M}$ for $\mathbf{q}^2 \ll 1$.

One may reproduce the correct behavior at *all* energies by using a definition in momentum space:

$$\Delta f_{\mathbf{j}} \equiv \sum_{\mathbf{n}} \frac{e^{i2\pi\mathbf{j}\cdot\mathbf{n}/N_x}}{N_x^{3/2}} \left(\frac{2\pi\mathbf{n}}{b_s N_x}\right)^2 \tilde{f}_{\mathbf{n}}, \tag{14}$$

where

$$\tilde{f}_{\mathbf{n}} \equiv \sum_{\mathbf{k}} \frac{e^{-i2\pi\mathbf{n}\cdot\mathbf{k}/N_x}}{N_x^{3/2}} f_{\mathbf{k}} \tag{15}$$

is the discrete Fourier transform of f. This yields

$$E(\mathbf{p}) = \frac{\mathbf{p}^2}{2M}, \tag{16}$$

by definition, at all energies.

The form of Eq. (12) has the advantage of being as local as possible, in the sense that the calculation of the Laplacian at point $\mathbf{j}$ requires input only from its nearest-neighbors $\mathbf{j} \pm \mathbf{e}_k$. This means that it can be performed very quickly on a computer. It should be kept in mind, however, that the memory layout in current computers is linear, such that nearest-neighbors in different directions can be physically very far from each other. This fact can affect performance considerably.

The form of Eq. (14), on the other hand, is as non-local as possible, but has the benefit of being closer to the continuum limit than any other implementation. References [74, 75] have analyzed the properties of these choices in the presence of interactions using a dynamical mean-field approach (see also Ref. [76])

This is a first glimpse at what is commonly referred to as "improvement". The action resulting from Eq. (14) is an improved version of that of Eq. (12), in the sense that it is closer to the continuum limit. In fact, Eq. (14) would lead to what we call a "perfect" action for the non-interacting system. We shall return to the issue of improved actions in Sec. 2.6. Other forms of improved dispersion relations, which in some sense interpolate between cases of Eq. (12) and Eq. (14), have been described in Ref. [77].

The issue of choosing a proper discretization for the temporal derivative ∂_τ requires some care. Indeed, as noted in Ref. [78], one should be careful when transferring fermion operators to the lattice. In particular, the generator of time translations, at finite temporal lattice spacing b_τ, will not be the discretized version of the Hamiltonian shown above; rather, we have

$$\psi_\tau - \psi_{\tau-1} = -(1 - B_\tau)\psi_{\tau-1}, \tag{17}$$

where

$$B_\tau \equiv \exp\left(-b_\tau H(\tau)\right), \tag{18}$$

for a general time-dependent Hamiltonian H. Therefore, the generator of translations is an effective Hamiltonian given by

$$b_\tau H^{\text{eff}}(\tau) = 1 - e^{-b_\tau H(\tau)}. \tag{19}$$

Taking this into account, the fermionic part of the Euclidean-time lattice action, in the absence of interactions, will be

$$S = \sum_{a,b} \psi_a^\dagger \left[K_0\right]_{ab} \psi_b \tag{20}$$

(we use collective indices a, b to denote points on the spacetime lattice), where

$$K_0 = \begin{pmatrix} 1 & 0 & 0 & 0 & \dots & B_0 \\ -B_0 & 1 & 0 & 0 & \dots & 0 \\ 0 & -B_0 & 1 & 0 & \dots & 0 \\ \vdots & \vdots & \vdots & \ddots & \vdots & \vdots \\ 0 & 0 & \dots & -B_0 & 1 & 0 \\ 0 & 0 & \dots & 0 & -B_0 & 1 \end{pmatrix}, \tag{21}$$

and where the entries are blocks of size $N_x^3 \times N_x^3$, with 1 being the unit matrix and $B_0 = \exp(-b_\tau(H_0 - \mu))$. Notice that this discretization amounts to a one-sided temporal derivative, which should be contrasted with the relativistic case, where a symmetric discretization is used.

Thus far, aside from the fact that we have only considered fermionic degrees of freedom in the problem, the formulation we have described is potentially general enough to cover a large number of problems in condensed-matter and nuclear physics. Unfortunately, once interactions are taken into account many of those problems are not easily tractable with current methods. Special techniques are needed to even begin to consider certain cases (e.g. systems with repulsive interactions) due to the appearance of the sign or signal-to-noise problem. We shall therefore restrict our attention even further whenever necessary, but we will return to signal-to-noise issues below, as it is an active topic of research in all areas.

In order to proceed, we shall focus on two-body interactions, such that in general,

$$H = \sum_{\mathbf{n},\mathbf{m}} \psi^\dagger_{\mathbf{n}} \left[H_0\right]_{\mathbf{n},\mathbf{m}} \psi_{\mathbf{m}} + \sum_{\mathbf{n},\mathbf{m},\mathbf{j},\mathbf{k}} \psi^\dagger_{\mathbf{n}} \psi^\dagger_{\mathbf{m}} \left[V_2\right]_{\mathbf{nmjk}} \psi_{\mathbf{j}} \psi_{\mathbf{k}} \tag{22}$$

In fact, this problem is already challenging. Indeed, while taking the exponential of a one-body operator is relatively easy, it is much harder to do so for a two-body operator. Similarly, the only field integral we know how to handle is the Gaussian case. It is for these reasons that auxiliary fields are introduced in order to deal with the interaction. Unfortunately, even for the simplest interactions there are cases where a sign problem arises, such as the case of the point-like repulsive potential. For a purely attractive potential, on the other hand, we may "decouple" the two-body interaction by using the Hubbard-Stratonovich "trick", which we now turn to.

2.3. Hubbard-Stratonovich transformations

Almost every lattice calculation is based on the fact that two-body interactions (from the Hubbard model to QCD) can be represented by mediation through bosonic fields. In QED this field is the physical photon field, in QCD it is the gluon field, and in theories with contact interactions (Hubbard model, Nambu-Jona Lasinio, Gross-Neveu, etc.) one uses a non-propagating "auxiliary field". This auxiliary field is introduced using the so-called Hubbard-Stratonovich (HS) transformation (in any of its many incarnations) in which the four-fermion operator of the interaction is effectively replaced by a path integral over a field ϕ that couples to a two-fermion operator [79, 80, 81]. Although the HS transformation is an extremely useful step toward putting the problem on a computer, it should be pointed out that there is an alternative that is particularly powerful for the case of contact interactions, namely the worm algorithm (see e.g. Refs. [82, 83, 84]).

To fix ideas we shall consider the case of spin-1/2 fermions with a contact interaction, such that the second term in Eq. (22) is given by

$$V = g \sum_{\mathbf{n}} \psi^\dagger_{\mathbf{n},\uparrow} \psi_{\mathbf{n},\uparrow} \psi^\dagger_{\mathbf{n},\downarrow} \psi_{\mathbf{n},\downarrow} \,. \tag{23}$$

As mentioned above, we will focus on time-independent potentials, such that we may evaluate the above expression at any time slice τ. The HS transformation is based on the fact that, at each point $a = \mathbf{n}, \tau$ in spacetime, we may write

$$e^{b_\tau g \psi^\dagger_{a,\uparrow}\psi_{a,\uparrow}\psi^\dagger_{a,\downarrow}\psi_{a,\downarrow}} = \frac{1}{\sqrt{2\pi}} \int_{-\infty}^{\infty} d\phi \; e^{-\frac{\phi^2}{2} - \phi\sqrt{b_\tau g}(\psi^\dagger_{a,\uparrow}\psi_{a,\uparrow} + \psi^\dagger_{a,\downarrow}\psi_{a,\downarrow})}. \tag{24}$$

A discrete version is also available:

$$e^{b_\tau g \psi^\dagger_{a,\uparrow}\psi_{a,\uparrow}\psi^\dagger_{a,\downarrow}\psi_{a,\downarrow}} = \frac{1}{2} \sum_{\phi=\pm 1} e^{-\phi\sqrt{b_\tau g}(\psi^\dagger_{a,\uparrow}\psi_{a,\uparrow} + \psi^\dagger_{a,\downarrow}\psi_{a,\downarrow})}, \tag{25}$$

and a continuous but compact form:

$$e^{b_\tau g \psi^\dagger_{a,\uparrow}\psi_{a,\uparrow}\psi^\dagger_{a,\downarrow}\psi_{a,\downarrow}} = \frac{1}{2\pi} \int_{-\pi}^{\pi} d\phi \; e^{-\sin(\phi)\sqrt{b_\tau g}(\psi^\dagger_{a,\uparrow}\psi_{a,\uparrow} + \psi^\dagger_{a,\downarrow}\psi_{a,\downarrow})}. \tag{26}$$

Implementing an HS transformation, the partition function becomes

$$\mathcal{Z} = \int \mathcal{D}\phi \mathcal{D}\psi^\dagger \mathcal{D}\psi \; \rho[\phi] e^{S[\phi,\psi^\dagger,\psi]}, \tag{27}$$

where the function $\rho[\phi]$ represents a contribution whose form depends on the specific choice of HS transformation. For these three possibilities (by no means an exhaustive list), we have

$$\rho[\phi] = \begin{cases} \prod_{\mathbf{n}} e^{-\frac{1}{2}\phi^2_{\mathbf{n}}} & \text{Continuous, unbounded (Refs. [79, 80])} \\ \prod_{\mathbf{n}} (\theta(-\pi + \phi_{\mathbf{n}})\theta(\pi - \phi_{\mathbf{n}})) & \text{Continuous, bounded (Refs. [85, 77])} \\ \prod_{\mathbf{n}} (\delta_{\phi_{\mathbf{n}},1} + \delta_{\phi_{\mathbf{n}},-1}) & \text{Discrete (Ref. [81]).} \end{cases}$$

The fermionic part of the Euclidean-time lattice action will be

$$S = \sum_{a,b} \psi^\dagger_a \left[K[\phi]\right]_{ab} \psi_b, \tag{28}$$

and the dynamics of the fermions is fully specified by the matrix K, which has a general structure given by

$$K[\phi] = \begin{pmatrix} 1 & 0 & 0 & 0 & \dots & B_{N_\tau}[\phi] \\ -B_1[\phi] & 1 & 0 & 0 & \dots & 0 \\ 0 & -B_2[\phi] & 1 & 0 & \dots & 0 \\ \vdots & \vdots & \vdots & \ddots & \vdots & \vdots \\ 0 & 0 & \dots & -B_{N_\tau-2}[\phi] & 1 & 0 \\ 0 & 0 & \dots & 0 & -B_{N_\tau-1}[\phi] & 1 \end{pmatrix} \tag{29}$$

where the entries are blocks of size $N_x^3 \times N_x^3$. Notice that the structure of this matrix is such that each block column (and row) corresponds to a particular temporal slice. It should be clear from the above that the derivative with respect to imaginary time that appears in the action is represented here as a one-sided difference. Also clear in this equation is the anti-periodic boundary condition along the time direction. In fact,

for ground-state studies, the upper-right block B_{N_τ} is in principle at our disposal, as it merely implements the boundary condition in the time direction, which is infinitely long at zero temperature. For instance, Refs. [86, 87, 88] use open boundary conditions, i.e. $B_{N_\tau} \equiv 0$; we shall elaborate on this choice in the Algorithms section.

The form of the B_k matrices, which in general are functions of ϕ, depends on the form of the interaction as well as on the choice of HS transformation. We shall see a specific example below.

Since the resulting action is quadratic in the fermion fields, we are now in a position to perform the path integration over the fermion fields, which leads to

$$\mathcal{Z} = \int \mathcal{D}\phi \, \mathcal{P}[\phi], \tag{30}$$

where

$$\mathcal{P}[\phi] \equiv \rho[\phi] \det K[\phi] \tag{31}$$

is the probability of the specific configuration ϕ. Here and in the following we shall neglect overall multiplicative constants in partition functions whenever possible (e.g. when integrating out fermions or performing gaussian integrals of any kind). (Extensive explanations on gaussian integration over various fields and dimensions appear in Ref. [72])

This formulation, which results from the grand-canonical approach to quantum statistical mechanics, is the most natural one in connection with finite-temperature studies (where the length of the time direction is proportional to the inverse temperature) as well as with its relativistic counterpart.

2.4. The canonical approach

As particle number is conserved in non-relativistic quantum mechanics, it is often natural to start from the canonical ensemble, which leads to a formulation based on a Slater determinant trial wavefunction for N particles and leads to a "partition function" (technically this is not a partition function as we are not truly summing over all possible quantum states, but it is a kind of probability sum) of the form

$$\mathcal{Z}_N = \int \mathcal{D}\phi \, \mathcal{P}_N[\phi], \tag{32}$$

where

$$\mathcal{P}_N[\phi] \equiv \rho[\phi] \det K_N[\phi], \tag{33}$$

$$[K_N]_{\alpha\beta} = \langle \alpha | B_{N_\tau} \cdots B_3 B_2 B_1 | \beta \rangle, \tag{34}$$

and $|\alpha\rangle$, $\alpha = 1, ..., N$ are the single-particle states in the Slater determinant. One may define at most N_x^3 linearly independent single-particle states, such that $N = N_x^3$ is the maximum number of particles we may place on the lattice, as befits fermions. In general, however, one takes $N \ll N_x^3$ to avoid lattice spacing effects (we shall return to systematic effects in general in Sec. 6).

Ground-state properties are obtained by extrapolation from finite β (i.e. finite N_τ) to the $\beta \to \infty$ limit by fitting to analytic formulas. The performance of calculations and subsequent extrapolations in this approach depends strongly on the choice of the single-particle basis and trial wavefunctions. For example, Ref. [89] uses functions that include some degree of pairing correlations, as does Ref. [90], while Ref. [91] uses simple Slater determinants of free-particle states.

These two formulations (the canonical and the grand canonical of the previous sections) are of course related in more than one way, starting from the fact that the matrices B_k that enter the imaginary time propagation have exactly the same form given the choice of dispersion relation and HS transformation. In the Algorithms section we shall elaborate on the differences and similarities between these two approaches.

As a particular example, if we choose the discrete form of the HS transformation, then

$$[B_k]_{\mathbf{n},\mathbf{n}'} = [\mathcal{K}\mathcal{V}_k]_{\mathbf{n},\mathbf{n}'}, \tag{35}$$

where the kinetic-energy factor is diagonal in momentum space and given by

$$[\mathcal{K}]_{\mathbf{p},\mathbf{p}'} = e^{-b_\tau(p^2/(2M)-\mu)}\delta_{\mathbf{p},\mathbf{p}'} \tag{36}$$

and the potential-energy factor is diagonal in coordinate space and reads

$$[\mathcal{V}_k]_{\mathbf{n},\mathbf{n}'} = (1+\sqrt{C}\phi(k,\mathbf{n}))\delta_{\mathbf{n},\mathbf{n}'}. \tag{37}$$

where $C = e^{b_\tau g} - 1$. (Notice that if g is negative, which corresponds to a repulsive interaction, then C is negative as well, and its square root is complex. This brings about the sign problem, as mentioned before.)

As the path integral is to be performed over $\phi(k,\mathbf{n})$, the actual form of the operator $\mathcal{V}_k$ will obviously vary wildly throughout a calculation. The operator $\mathcal{T}$, on the other hand, is constant. Therefore, in practice, $\mathcal{T}$ is computed only once at the beginning of a calculation and stored in memory. Furthermore, it is best to compute it in momentum space where it is diagonal (it is a fully dense matrix in coordinate space) and apply it as needed by using fast Fourier transforms (FFT).

The strategy of using FFT to apply operators that are non-local in coordinate space but diagonal in momentum space, is commonly referred to as "Fourier acceleration" (see e.g. [92, 93, 94, 95]). To the uninitiated this may appear to be a ridiculously convoluted way to proceed. Why not do everything in coordinate space instead of switching back and forth? The reason is that applying a dense matrix of dimension $M \times M$ to a vector is an operation whose computational cost scales as M^2, whereas using FFT for this purpose changes the scaling to $M \log M$. Moreover, modern FFT libraries, such as FFTW [96] are so advanced that their performance is very difficult to improve, even in cases where the matrix in question is somewhat sparse in its coordinate-space representation (e.g. when using a nearest-neighbor finite-difference formula for the momentum operator).

2.5. A comment on many-body forces

As mentioned above, in this article we restrict ourselves to two-body forces. Higher-body forces, however, play a crucial role in nuclear physics and should therefore be somehow accounted for. In Ref. [39] a strategy is used to include interactions beyond two-body in a perturbative fashion.

If the perturbative approach is justified, i.e. if the couplings g_n (assume $n > 2$) to the interaction operators $\hat{H}_n$ are indeed much smaller for the higher-body forces in question than for the two-body sector, then one may expand the action around vanishing g_n, such that the partition function becomes

$$\mathcal{Z} = \mathcal{Z}|_{g_n=0,n>2} + \sum_{n>2} g_n \left.\frac{\partial \mathcal{Z}}{\partial g_n}\right|_{g_n=0} + \frac{1}{2}\sum_{n,m>2} g_n g_m \left.\frac{\partial^2 \mathcal{Z}}{\partial g_n \partial g_m}\right|_{g_n,g_m=0} + \ldots. \tag{38}$$

In practice this is performed introducing sources coupled to one-fermion operators. The evaluation of observables will therefore include propagators reflecting the insertion of the interaction. A different way to proceed is to attempt to perform an HS transformation on the many-body interaction in question. Unfortunately this introduces a sign problem in almost any case of interest.

2.6. Improved Actions & Transfer Matrices

At this point we have presented the various steps necessary to connect the formalism of finite-temperature many-body quantum mechanics with the expressions amenable to numerical calculation. Before moving on to specific algorithms to sample the probability measure, and then to the problem of computing observables, it is worth pointing out a recent development which modifies the zero-range Hamiltonian presented above in order to allow faster approach the continuum limit. This represents a kind of improved action. Improved observables can also be defined using the same methods, as we shall see in a later section.

The starting point is the transfer matrix $\mathcal{T}$. By definition, as we saw above,

$$\mathcal{T} = \exp(-b_\tau \hat{H}) \simeq \int d\phi(k) \hat{\mathcal{K}} \hat{\mathcal{V}}_k[\phi] + O(b_\tau^2), \tag{39}$$

where $\mathcal{K}$ and $\mathcal{V}_k$ are as in Eqs. (36) and (37), respectively, and we have set $\mu = 0$. In order to reduce lattice-spacing effects in non-relativistic systems Refs. [97, 86] employed the following strategy. One may promote the constant C in Eq. (37) to an operator $C(\hat{p})$ that is diagonal in momentum space, such that a more general HS transformation is defined. In order to fix the form of the function $C(p)$, one parametrizes its form using a convenient set of basis functions $\mathcal{O}_{2n}(\mathbf{p})$,

$$C(\mathbf{p}) = \frac{4\pi}{M} \sum_{n=0}^{N_\mathcal{O}-1} C_{2n} \mathcal{O}_{2n}(\mathbf{p}) \,, \tag{40}$$

and then diagonalizes the transfer matrix in the two-particle subspace of the Fock space, which is given in the momentum representation by

$$\mathcal{T}_2(\boldsymbol{p}_\uparrow \boldsymbol{p}_\downarrow; \boldsymbol{q}_\uparrow \boldsymbol{q}_\downarrow) = \tag{41}$$

$$e^{-\frac{b_\tau T(p)}{2}} \left[\delta_{\boldsymbol{p}_\uparrow \boldsymbol{q}_\uparrow} \delta_{\boldsymbol{p}_\downarrow \boldsymbol{q}_\downarrow} + \frac{\sqrt{C(\boldsymbol{p}_\uparrow - \boldsymbol{q}_\uparrow)} \sqrt{C(\boldsymbol{p}_\downarrow - \boldsymbol{q}_\downarrow)}}{2V} \delta_{\boldsymbol{p}_\uparrow + \boldsymbol{p}_\downarrow, \boldsymbol{q}_\uparrow + \boldsymbol{q}_\downarrow} \right] e^{-\frac{b_\tau T(q)}{2}} \tag{42}$$

where $V = N_x^3$ is the lattice volume and $T(k) = (\boldsymbol{k}_\uparrow^2 + \boldsymbol{k}_\downarrow^2)/(2M)$.

The exact eigenvalues of the transfer matrix corresponding to a given choice of scattering parameters is given by Lüscher's formula [98, 99]:

$$p \cot \delta_0(p) = -\frac{1}{a_S} + \frac{1}{2} r_0 p^2 + O(p^4) = \frac{1}{\pi L} \mathcal{S}(\eta) \tag{43}$$

where a is the scattering length, r is the effective range, $\eta \equiv \frac{pL}{2\pi}$, and

$$\mathcal{S}(\eta) \equiv \lim_{\Lambda \to \infty} \sum_{\mathbf{n}} \frac{\Theta(\Lambda^2 - \mathbf{n}^2)}{\mathbf{n}^2 - \eta^2} - 4\pi\Lambda, \tag{44}$$

where the sum is over all 3D integer vectors.

In the case of the unitary limit, where by definition

$$p \cot \delta_0(p) \equiv 0, \tag{45}$$

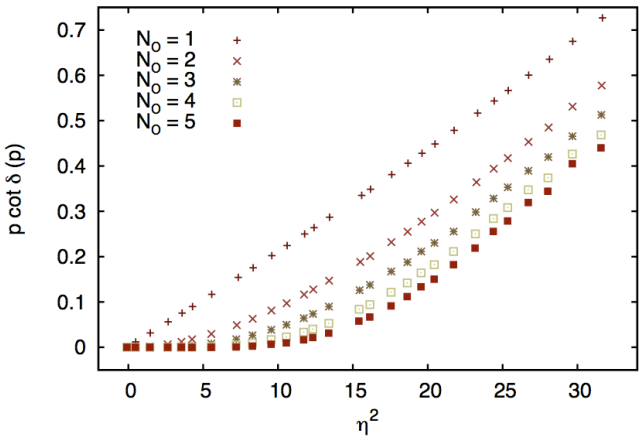

Figure 1. (Color online) Plot of $p \cot \delta(p)$ as a function of $\eta^2 = E_2/p_0^2$ (where $p_0 \equiv 2\pi/L$), for $N_x = 20$, $b_\tau = 0.05$, and levels of improvement $N_{\mathcal{O}} = 1 - 5$, for a Galilean invariant definition of the transfer matrix.

the above procedure yields considerable improvement in the approach to the continuum. Indeed, with a single coefficient C_0 one may tune the scattering length a, but the effective range r remains finite due to lattice-spacing artifacts (systematic effects will be discussed in more detail in Sec. 6). Naturally, by introducing more parameters one may tune the effective-range expansion in Eq. (43) to higher accuracy (see Fig. 1), thus systematically eliminating the need for extrapolations to the dilute limit and leaving only finite-volume effects unaccounted for.

Thus, tuning to the unitary point requires knowledge of the roots of $S(\eta)$. The first few roots are quoted in the Appendix. The result of the fit is shown in Table 1, for various improvement levels.

Table 1. Results of fitting the coefficients C_n to the low-energy spectrum of the two-body problem at resonance, in a box of side $N_x = 16$, for an imaginary time step $b_\tau = 0.05$, in lattice units.

$N_{\mathcal{O}}$	C_0	C_1	C_2	C_3	C_4
1	0.68419	–	–	–	–
2	0.53153	0.07896	–	–	–
3	0.49278	0.04366	0.01807	–	–
4	0.47217	0.03711	0.00784	0.00467	–
5	0.45853	0.03331	0.00718	0.00132	0.00129

3. Algorithms

In the previous section we outlined the general strategy that is typically followed to write down a two-body Hamiltonian in a form that can be treated with Monte Carlo methods. Our main development was expressing the partition function as a sum over auxiliary-field configurations:

$$\mathcal{Z} = \int \mathcal{D}\phi \, \mathcal{P}[\phi], \tag{46}$$

where $\mathcal{P}[\phi]$ generally involves the determinant of a large matrix whenever fermions are involved.

Once a suitable probability measure $\mathcal{P}[\phi]$ has been chosen, one faces the task of constructing an efficient method to sample uncorrelated field configurations that obey such a probability. Here, the importance of the word "efficient" should not be underestimated. Indeed, the possibility of evaluating a path integral stochastically is a remarkable step forward given the size of the domain of integration, but stochastic integration of quantum systems would not be viable without methods for fast sampling of $\mathcal{P}[\phi]$. This consideration is quite general, applying to relativistic as well as non-relativistic problems. Indeed, none of the endeavors of the Lattice QCD community would be possible without fast sampling methods. In this section we describe some of these methods, specifically for the case of non-relativistic systems. The problem at hand is equivalent to that of constructing an efficient random number generator, where the output is not just one number but a field defined in space-time.

Among the methods available to tackle this problem, one may identify two large classes: the so-called heat-bath methods, which allow for the direct generation of uncorrelated samples; and Markov-chain methods, based on the Metropolis algorithm [100]. While the former are extremely useful when studying for instance pure gauge theories [101, 102, 103, 104], their use is much more limited in the case of theories that involve dynamical fermions due to the complexity (non- linearity and non-locality) of the fermion determinant present in $\mathcal{P}[\phi]$. As we shall see, however, heat-bath approaches are still useful for non-relativistic fermion theories in certain formulations. Markov-chain approaches, on the other hand, are the most popular and generally viable when dealing with fermions (as long as there is no sign problem), and we shall therefore discuss them first.

3.1. Determinantal Monte Carlo

One the simplest methods to sample a non-trivial fermionic probability is known by the name of Determinantal Monte Carlo (DMC). In this algorithm, one generates a sequence of samples of the auxiliary field ϕ (the Markov chain) by performing localized changes, typically of random magnitude affecting a random set of locations. The new configuration, ϕ_{new}, is then accepted or rejected according to the Metropolis algorithm, i.e. with a probability of acceptance given by

$$p = \min\left(1, \frac{\mathcal{P}[\phi_{\text{new}}]}{\mathcal{P}[\phi_{\text{old}}]}\right). \tag{47}$$

where $\mathcal{P}[\phi] = \det K[\phi]$.

As successive configurations are strongly correlated with each other, snapshots of the field should be taken at sufficiently long intervals along the chain. Such a process of decorrelation can be time consuming, depending on the proximity to critical points

[]. The minimal requirements for this algorithm to function and yield the correct probability measure are ergodicity and detailed balance (though technically a weaker condition is enough, see e.g. Ref. [105] for a nice overview). Ergodicity implies that long enough chains will eventually touch every point in the space of possible configurations. Detailed balance, i.e. ensuring that a given update has the same probability as the reverse process, implies that the Markov chain has $\mathcal{P}[\phi]$ as a fixed point.

When moving from one configuration to the next, it is possible in some cases to update clusters of points at a time, as explored many years ago in the context of the Ising model [106, 107, 108]. However, such attempts to take long random steps in configuration space in our case will in general, though not always, result in a low probability of acceptance. One is therefore forced to take relatively small steps. On the other hand, taking very small steps should be avoided as well, as they yield high acceptance but slow decorrelation and are therefore very inefficient. The rule of thumb is then to compromise by choosing updates such that the acceptance rate is in the range 40-60%.

The DMC method is not only among the simplest, but is also one of the oldest and remains in wide use (see e.g. [109] for a recent use of DMC); it is also very effective, but unfortunately not particularly efficient. The main drawback of the "plain" version of DMC presented here is that localized updates of the field represent a huge cost from the computational point of view. Indeed, strongly correlated systems are generally not amenable to global modifications of the field, and the (integrated) size of the randomly updated regions generally does not scale up with the volume of the system. As a consequence, the cost of a full update (a sweep), which is a measure of the cost of obtaining a useful configuration, scales as $NN_\tau^2V^3$, where N is the number of particles, N_τ is the number of lattice points in the imaginary time direction, and $V = N_x^3$ is the spatial volume. This estimate results from the evolution of N particles in imaginary time over N_τ steps, with a cost per step equal to that of dense matrix-vector multiplication, which on a basis of size V scales as V^2. The cost of local updates contributes an extra factor of $N_\tau V$, because the auxiliary field lives in all of spacetime, which yields the final result. This estimate does not account for the possibility of Fourier acceleration, in which case the cost of a time step is proportional to $V \log V$, resulting in a cost per sweep of $NN_\tau^2V^2 \log V$.

3.2. Hybrid Monte Carlo

As of this writing, the use of Hybrid Monte Carlo (HMC) in non-relativistic physics is surprisingly scarce, both at zero as well as finite temperature. While this powerful algorithm was developed many years ago in the field of Lattice QCD [110, 111], its application to strongly correlated systems in other fields, in particular condensed matter and low-energy nuclear physics is still in its infancy (with some exceptions, see Ref. [77, 28]).

The HMC method, as DMC, is based on the generation of a Markov sequence of configurations that are accepted or rejected as dictated by the Metropolis algorithm. The fundamental difference between DMC and HMC (in its various forms) is that the latter enables *global* updates of the field, which reduces the cost per sweep to $NN_\tau V^2$, or $NN_\tau V \log V$ when Fourier acceleration is possible. This dramatic improvement is accomplished by introducing molecular dynamics (MD) into the updating procedure in the following way.

Given the probability measure $\mathcal{P}[\phi]$ and corresponding "effective" action

$$S_{\text{eff}}[\phi] \equiv -\log \mathcal{P}[\phi], \tag{48}$$

one introduces a fictitious gaussian-distributed momentum field π, which modifies the partition function only by a multiplicative constant, i.e. in a way that is immaterial to the dynamics of the system:

$$\mathcal{Z} = \int \mathcal{D}\phi \mathcal{P}[\phi] \to \int \mathcal{D}\phi \mathcal{D}\pi \mathcal{P}[\phi, \pi], \tag{49}$$

where

$$\mathcal{P}[\phi, \pi] = \exp\left(-\sum_{\mathbf{n},\tau} \frac{\pi^2_{\mathbf{n},\tau}}{2}\right) \mathcal{P}[\phi] = \exp\left(-\mathcal{H}_{\text{MD}}\right), \tag{50}$$

and

$$\mathcal{H}_{\text{MD}} \equiv \sum_{\mathbf{n},\tau} \frac{\pi^2_{\mathbf{n},\tau}}{2} + S_{\text{eff}}[\phi]. \tag{51}$$

Since we have not modified the true dynamics of the problem, this new probability $\mathcal{P}[\phi, \pi]$ is physically equivalent to the original one. The reason it is advantageous to work with this enlarged problem is that one may use MD as the updating strategy to explore configuration space. Taking a gaussian distributed π and any choice of ϕ as the initial conditions, one solves the classical evolution equations dictated by $\mathcal{H}_{\text{MD}}$:

$$\begin{aligned} \dot{\phi}_{\mathbf{n},\tau} &= \pi_{\mathbf{n},\tau}, \\ \dot{\pi}_{\mathbf{n},\tau} &= F_{\mathbf{n},\tau}[\phi] \equiv -\frac{\delta S_{\text{eff}}[\phi]}{\delta \phi_{\mathbf{n},\tau}}, \end{aligned} \tag{52}$$

where the dots indicate a derivative with respect to the fictitious MD time t_{MD}. Notice that these equations are global, i.e. they affect each and every point in space-time, such that upon integration along a trajectory of length $T_{\text{MD}} \sim 1$ one obtains a fully updated field configuration, i.e. one has performed a sweep. If these equations were integrated exactly, the fictitious energy given by $\mathcal{H}_{\text{MD}}$ would be conserved, and the probability of acceptance of any trajectory would be exactly 1. It is this combination of MD with the Metropolis algorithm that gives the "Hybrid" in HMC. In practice, integrators are precise but not exact, such that a Metropolis step, comparing the probabilities at the beginning and at the end of the trajectory, is needed to guarantee that the correct probability distribution is being sampled. Resampling of the fictitious momentum π at the beginning of each trajectory is needed to actually perform the integral over π that appears in Eq. (49). This also takes the random walk in a new direction and into a different MD classical orbit, which favors faster decorrelation.

In order to maintain detailed balance, as required by the Metropolis algorithm, the MD equations (52) must be integrated in a reversible and area-preserving fashion (see e.g. Refs. [110, 111, 105]). This is accomplished by implementing a symplectic and symmetric integrator, such as the leap-frog algorithm, or more sophisticated approaches like the Omelyan integrators [112].

It should be stressed that, in contrast to the DMC algorithm, the current form of HMC applies only to the case in which the field ϕ is continuous. This is a prerequisite if classical differential equations are to be used for the MD evolution, and it is somewhat unfortunate, as there are a variety of formulations that rely on discrete fields, which have the obvious advantage of requiring significantly less storage space than their continuous counterparts.

3.3. Pseudofermions and connection to the finite temperature case

One of the most common versions of the HMC algorithm, used routinely in Lattice QCD, utilizes the so-called pseudofermion fields χ to represent the determinant via the following relation:

$$\det M[\phi] \propto \int \mathcal{D}\chi^\dagger \mathcal{D}\chi \exp\left(-\chi^\dagger M^{-1}[\phi]\chi\right), \tag{53}$$

where we assume that all the indices are contracted in the exponent on the right-hand side, and it is assumed that the dynamics encoded in M is such that the gaussian integral is well defined. In practice, this integral is evaluated stochastically, exploiting its gaussian form. The name "pseudofermion" arises from the fact that these are bosonic complex-valued fields whose dynamics is given by M^{-1}, which satisfies antiperiodic boundary conditions in the time direction. To our knowledge, pseudofermions have never been used in non-relativistic ground-state calculations, possibly because in that case the determinants are substantially smaller than in the finite-temperature and/or relativistic cases, such that an exact calculation of $\det M$ is feasible and even convenient in comparison.

In this case the MD force takes the form

$$F_{\mathbf{n},\tau}[\phi] = \left[\chi^\dagger M^{-1}[\phi]\right] \frac{\delta M[\phi]}{\delta \phi_{\mathbf{n},\tau}} \left[M^{-1}[\phi]\chi\right], \tag{54}$$

where again all the indices are implicitly contracted. It is easy to see that a fermion sign problem will ensue unless M is positive semidefinite. The latter happens, in particular, in cases with an even number of flavors, where (under certain circumstances, e.g. spin symmetry) we may define a matrix K such that $\det M = \det K^\dagger K$.

A less common version of the HMC algorithm combines the advantages of both the DMC and HMC algorithms, without using pseudofermions, resulting in the so-called Determinantal Hybrid Monte Carlo algorithm. The idea behind this approach is to make use of the fact that

$$\det M = \det(1 + \mathcal{U}[\phi])^{N_f}, \tag{55}$$

where

$$\mathcal{U}[\phi] = B_{N_\tau} \cdots B_3 B_2 B_1 \tag{56}$$

(see Sec. 2).

Notice that the determinant on the left-hand side of Eq. (55) is over a spacetime matrix, whereas the one on the right-hand side is purely spatial. The fact that this simplification is possible is directly related to the absence of backward temporal propagation in non-relativistic theories.

The zero-temperature version of this discussion is directly connected to the use of a Slater determinant $|\alpha_0\rangle$ as the starting point or "guess" for the ground-state wavefunction, which we mentioned in Section 2. In that case,

$$\mathcal{Z} = \int \mathcal{D}\phi \det(\mathcal{U}[\phi])^{N_f}, \tag{57}$$

where the determinant is to be taken over the space generated by the single-particle (s.p.) orbitals φ_j that make up $|\alpha_0\rangle$, such that

$$F_{\mathbf{n},\tau}[\phi] = N_f \operatorname{tr}\left[\mathcal{U}[\phi]^{-1} \frac{\mathcal{U}[\phi]}{\delta \phi_{\mathbf{n},\tau}}\right] \tag{58}$$

where, as with the determinant, both the trace and the inverse are to be interpreted as restricted to the subspace generated by the s.p. orbitals φ_j.

3.4. Heat-bath approach

An interesting recent development in the field of lattice fermion calculations concerns exploiting the fact that the non-relativistic ground-state problem can be formulated in a way that the fermion determinant is identically equal to 1, for all the field configurations [86, 87, 88, 89, 97, 113]. Indeed, as mentioned in the Introduction, ground-state calculations give us the freedom to choose the form of the boundary condition in the time direction, and in particular we may choose an open boundary condition, such that the dynamics is governed by the triangular matrix

$$K[\phi] = \begin{pmatrix} 1 & 0 & 0 & 0 & \dots & 0 \\ -B_1 & 1 & 0 & 0 & \dots & 0 \\ 0 & -B_2 & 1 & 0 & \dots & 0 \\ \vdots & \vdots & \vdots & \ddots & \vdots & \vdots \\ 0 & 0 & \dots & -B_{N_\tau-2} & 1 & 0 \\ 0 & 0 & \dots & 0 & -B_{N_\tau-1} & 1 \end{pmatrix}. \tag{59}$$

Not only is $\det K = 1$, but the triangular form also gives us direct access to the inverse:

$$K^{-1}[\phi] = \begin{pmatrix} 1 & 0 & 0 & 0 & \dots & 0 \\ B_1 & 1 & 0 & 0 & \dots & 0 \\ B_2B_1 & B_2 & 1 & 0 & \dots & 0 \\ \vdots & \vdots & \vdots & \ddots & \vdots & \vdots \\ \prod_{k=1}^{N_\tau-1} B_k & \dots & \dots & \dots & B_{N_\tau-1} & 1 \end{pmatrix}. \tag{60}$$

This constitutes a case in which, trivially, one can sample uncorrelated field configurations directly according to the relevant probability measure, and it thus falls into the category of heat-bath approaches. This is a dramatic simplification of the original problem that comes with advantages and disadvantages.

On the positive side, a constant probability measure means that the cost of generating configurations is essentially insensitive to the number of particles and the size of the lattice, depending only on the speed of the uniform random number generator of choice. Field generation in this approach is therefore instantaneous compared to the other methods. Furthermore, a single set of configurations and propagators may be generated and then used for any number of observables desired. In addition, a constant probability implies no sign problem, regardless of spin asymmetry, nature of the interaction (attractive/repulsive, two-body, three-body, etc.), etc. This approach therefore constitutes an intriguing possibility for ground-state studies of a variety of systems in condensed-matter and nuclear physics, where the sign problem has been a major roadblock to progress.

On the negative side, this formulation is restricted to zero temperature, where one may legitimately ignore the (anti-periodic) boundary condition in the time direction. Furthermore, a constant probability implies that importance sampling is not possible: all the configurations are in principle equally important. In practice, the sign problem reappears here in the form of a statistical "overlap problem": the random configurations may not have much weight for the observable of interest. Using a very large number of configurations ($\sim 10^8$) and a sophisticated statistical analysis (see Sec. 5) it is still possible to perform calculations and obtain results with unprecedented precision.

Perhaps one of the main advantages of this method is not that it "solves" the sign problem, but rather that it replaces it with a new problem that we have a better

chance to tackle, in particular if aided by physical insight into the system at hand.

3.5. Open-ended imaginary-time evolution, re-weighting and branching random walks

Extracting ground-state properties entails performing calculations for β as large as possible. We will return to the issue of extrapolating to the $\beta \to \infty$ limit from finite β data below. It is important to underline, however, that serious technical difficulties arise at large β. As explained most recently in Ref. [97, 113], and as we review below, an interval of exponential approach to the asymptotic ground-state properties (even for simple observables such as the energy) is typically followed by a dramatic deterioration in the signal-to-noise ratio, which may render the whole extrapolation effort dubious, or at least quite complicated.

The algorithms explained in the previous subsections generally involve fixing the spatial and temporal extents of the lattice, followed by sampling configurations of the auxiliary field defined on that lattice. Notice that the heat-bath algorithm, however, does not require a temporal direction of fixed extent, as the probability measure does not depend on the size of the lattice in any way.

There is a different set of algorithms that have been in use since at least the mid-1990's, which allow for an open-ended temporal direction, such that in practice it has been possible to reach temporal extents a factor of at least 2 or 3 larger than with the methods outlined above. Clearly, following this strategy is at odds with the common practice of saving auxiliary field configurations of fixed size. These are, however, powerful algorithms that have largely remained unknown in various communities, and so we wish to outline them here.

The starting point is, as above, the factorization and Hubbard-Stratonovich transformation of the transfer matrix:

$$\mathcal{T}_t = \int \mathcal{D}\phi_t \; \mathcal{T}[\phi_t], \tag{61}$$

where typically we have two (or more) flavors, such that,

$$\mathcal{T}[\phi_t] = \mathcal{T}_\uparrow[\phi_t]\mathcal{T}_\downarrow[\phi_t]. \tag{62}$$

This is valid for each temporal slice, and we may therefore take a "guess" wavefunction $|\Psi_0\rangle$ and apply a sequence of $\mathcal{T}$'s for a given spacetime field configuration ϕ. The problem remains, of course, of summing over all possible ϕ fields in order to recover the physics we are interested in. Should we choose to pick configurations purely randomly, we would obtain the heat-bath algorithm of the previous section. As mentioned before, this may lead to substantial statistical noise.

The idea we wish to outline here, which first appeared in Refs. [114, 115], is essentially what in certain areas is called "re-weighting", but with a crucial twist. Instead of using a flat probability measure, one may assign a weight to the auxiliary field configurations; the crucial point is in introducing this weight by defining a probability in which the temporal dependence factorizes completely. This property of factorization is trivially true for the heat-bath method, but is certainly not satisfied for the DMC, DHMC or HMC approaches, where all of spacetime is inextricably linked into the fermion determinant. In this fashion, one may perform an open-ended random walk in imaginary time.

The first step is to consider not a single Slater-determinant wavefunction but a sum of them, all with equal probability, making up the initial guess for the ground

state $|\Psi_0\rangle$:

$$|\Psi_0\rangle = \sum_{k=1}^{N_w} |\varphi_k^0\rangle. \tag{63}$$

The imaginary-time evolution from step t to $t+1$ is then carried out on each Slater determinant by applying the HS-transformed transfer matrix:

$$|\varphi_k^{t+1}\rangle = \int \mathcal{D}\phi_{t+1} \mathcal{T}[\phi_{t+1}] |\varphi_k^t\rangle. \tag{64}$$

In principle, in the above path integral, all the field configurations at that time slice, ϕ_{t+1}, are equally important. To improve the efficiency of the temporal evolution we introduce the re-weighting strategy mentioned above.

For each evolved Slater determinant state (what is often called a "walker") $|\varphi_k^t\rangle$ we define an importance function

$$O_T(\varphi_k^t) = \langle \Psi_T | \varphi_k^t \rangle. \tag{65}$$

With this weight we can now write the imaginary-time evolution as

$$|\psi_k^{t+1}\rangle = \int \mathcal{D}\phi_{t+1} \mathcal{P}_k[\phi_{t+1}] \mathcal{T}[\phi_{t+1}] |\psi_k^t\rangle. \tag{66}$$

where we have defined a modified walker

$$|\psi_k^t\rangle = O_T(\varphi_k^t) |\varphi_k^t\rangle \tag{67}$$

and a probability

$$\mathcal{P}_k[\phi_{t+1}] = \frac{O_T(\varphi^{t+1})}{O_T(\varphi^t)}, \tag{68}$$

which depends on the initial and final states $|\varphi^{(t)}\rangle$ and $|\varphi^{(t+1)}\rangle$, respectively.

At this stage, the algorithm appears to be reduced to sampling the auxiliary field ϕ_{t+1} with the probability $\mathcal{P}_k[\phi_{t+1}]$, and thus construct the evolution operator for the modified walkers. It can be shown, as in the cases we discussed before, that in the presence of an equal number of fermions for each flavor (and for an even number of flavors) this probability is positive semidefinite, and this holds in particular for a particle-projected BCS state [90]. At the end of the problem the unmodified walkers are recovered simply by dividing by the relevant O_T.

There is however a problem in that $\mathcal{P}_k$ is not normalized, and typically importance sampling will introduce a normalization automatically (which is another way of saying that a normalized probability is required). We are therefore forced to consider the expression

$$|\psi_k^{t+1}\rangle = N_k^{t+1} \int \mathcal{D}\phi_{t+1} \bar{\mathcal{P}}_k[\phi_{t+1}] \mathcal{T}[\phi_{t+1}] |\psi_k^t\rangle, \tag{69}$$

where

$$\bar{\mathcal{P}}_k[\phi_t] \equiv \frac{\mathcal{P}_k[\phi_t]}{N_k^t} \tag{70}$$

and

$$N_k^t = \int \mathcal{D}\phi_t \mathcal{P}_k[\phi_t] \tag{71}$$

is of course the normalization of $\mathcal{P}_k[\phi_t]$.

The evolution in imaginary time then proceeds by obtaining N_s samples of ϕ_{t+1} that obey the normalized probability measure $\bar{\mathcal{P}}_k$, and using the stochastic estimate of the path integral as the evolution operator:

$$\int \mathcal{D}\phi_{t+1} \bar{\mathcal{P}}_k[\phi_{t+1}] \mathcal{T}[\phi_{t+1}] \simeq \frac{1}{N_s} \sum_{q=1}^{N_s} \mathcal{T}[\phi^q_{t+1}]. \tag{72}$$

The normalization constants N_k^t corresponding to each walker are separately accumulated in the so-called "weight" variables according to

$$w_k^{t+1} = N_k^{t+1} w_k^t, \tag{73}$$

with $w_k^0 \equiv 1$.

The calculation of the normalization is in general not trivial. However, as explained in Refs. [114, 115], this can be overcome by updating one lattice site at a time.

After a period of equilibration, i.e. for large enough t, one can expect to obtain an estimate of the ground state, which is given by

$$|\Psi_0\rangle \simeq \sum_k w_k^t |\varphi_k^t\rangle, \tag{74}$$

up to an overall normalization factor.

In practice, the weights of certain walkers will quickly grow after a few time steps, while others will decrease to zero. It is for this reason that the concept of "branching" is introduced. The idea is simple: every few steps in imaginary time, consider the possibility of randomly keeping or discarding some of the walkers. The number of steps (or equivalently the size of the time step) should be adjusted in such a way that roughly $40 - 60\%$ of the walkers are discarded at each instance. Of the walkers that remain, some of them are used to generate two or more new walkers, adjusting the number with a given algorithm, in such a way that the total number of walkers remains approximately constant throughout the calculation. At that point it is also important to re-orthonormalize the whole set of walkers to avoid stability issues. By allowing for the possibility of branching, one is essentially re-starting the calculation with a many-body wavefunction that is closer to the ground state than the original guess. In this way it is possible to evolve in imaginary time for much longer than with other algorithms.

4. Observables

4.1. Calculating the energy

The simplest observable to compute using lattice methods is the ground-state energy of a system. One method for doing so is to construct the N-body correlation function,

$$\mathcal{C}_N(\beta) = \frac{1}{\mathcal{Z}} \int \mathcal{D}\phi \mathcal{D}\psi^\dagger \mathcal{D}\psi e^{-S[\psi^\dagger,\psi,\phi]} \Psi_N^{(A)}(\beta) \Psi_N^{\dagger(B)}(0)\,, \tag{75}$$

where $\mathcal{Z}$ is the partition function, and the source (sink) is given by

$$\Psi_n^{(a)}(\tau) = \int dx_1 \cdots dx_n A^{(a)}(x_1 \cdots x_n) \psi_1(x_1) \cdots \psi_n(x_n)\,, \tag{76}$$

where $A^{(a)}$ is an N-body wavefunction and the fields ψ_i are chosen with the appropriate quantum numbers such that $\Psi_n^{(a)}$ has nonzero overlap with the state of interest. The simplest form for $\Psi_n^{(a)}$ is a product of non-interacting single-particle states, however, more sophisticated choices, for example including pairing correlations, may be incorporated into the wavefunction $A^{(a)}$ to have superior overlap with the ground state. This will be discussed in more detail in Sec. 5.

Upon integrating out the ψ fields we have

$$\mathcal{C}_N(\beta) = \frac{1}{\mathcal{Z}} \int \mathcal{D}\phi \mathcal{P}(\phi) \tilde{\mathcal{C}}(\phi,\beta)\,, \tag{77}$$

where

$$\tilde{\mathcal{C}}(\phi,\beta) = f(S_1(\phi,\beta), S_2(\phi,\beta), \cdots) \tag{78}$$

where f is a function of single- or multi-particle propagators, depending on the form of Ψ. This function should be properly (anti)symmetrized for (fermionic) bosonic fields. Using the simplest example of sources and sinks composed of single-particle states $|\alpha\rangle, |\beta\rangle$, f becomes a Slater determinant of single-particle propagators, so that $\tilde{\mathcal{C}} = \det S_{\alpha,\beta}$, where

$$S_{\alpha,\beta} = \langle \alpha | B_{N_\tau} \cdots B_3 B_2 B_1 | \beta \rangle\,, \tag{79}$$

and we reproduce the canonical partition function, Eq. 32. The form of the propagators in Eq. 79 may be recognized as a product of transfer matrices, $B_\tau = e^{-b_\tau \mathcal{H}}$, projected onto the chosen initial and final states.

One may insert a complete set of energy eigenstates into the correlation function, Eq. 75, to show that for a given Euclidean time β,

$$\begin{aligned} \mathcal{C}_N(\beta) &= \sum_{m,n} \langle \Psi_N^{(A)} | m \rangle \langle m | \prod_{\tau=1}^{\beta} e^{-b_\tau \mathcal{H}} | n \rangle \langle n | \Psi_N^{(B)} \rangle \\ &= Z_0 e^{-\beta E_0} + Z_1 e^{-\beta E_1} + \cdots\,, \end{aligned} \tag{80}$$

where $Z_a \equiv \langle \Psi_{src} | a \rangle \langle a | \Psi_{snk} \rangle$ is the overlap of the a-th energy eigenstate of the system with the chosen sources/sinks and E_a is the energy associated with that state. To extract the ground state, it is often useful to construct what is commonly called the effective mass,

$$m_{\text{eff}}(\beta) = \frac{1}{\Delta\beta} \ln \frac{\mathcal{C}(\beta)}{\mathcal{C}(\beta + \Delta\beta)} \underset{\beta\to\infty}{\longrightarrow} E_0 + \frac{Z_1}{Z_0} e^{-(E_1 - E_0)\beta} + \cdots \tag{81}$$

For sufficiently large $\beta \gg E_1 - E_0$, the ground state energy will dominate as excited state contributions are exponentially suppressed. By plotting this quantity as a

function of β, one looks for a plateau to indicate the elimination of excited states. The plateau region may then be fit to extract the ground state energy as well as a statistical uncertainty using standard methods.

One may also choose to use the thermodynamic definition of the energy, $E(\beta) \equiv -\frac{\partial \log \mathcal{Z}(\beta)}{\partial \beta}$. For the large-$\beta$ limit one obtains an expression similar to that derived for the correlator,

$$E(\beta) \underset{\beta\to\infty}{\longrightarrow} E_0 + b_E e^{-(E_1-E_0)\beta}, \tag{82}$$

where

$$b_E = \frac{Z_1}{Z_0}(E_1 - E_0). \tag{83}$$

Taking for example the canonical partition function obtained using a Slater determinant state Eq. (32), the observable calculated on each field configuration will be

$$\mathcal{O}_N(\beta) = E_N(\beta) = -\mathrm{Tr}\left[K_N^{-1}(\beta)\frac{\partial K_N(\beta)}{\partial \beta}\right]. \tag{84}$$

In Sec. 4.3 techniques for improving observables will be discussed, using this form of the energy as a first example.

As seen in Eqs. (81),(82), information about excited state energies is also available from these methods. Fortunately, there exists a vast literature on sophisticated techniques developed by the lattice QCD community which one may borrow to tackle the problem of extracting excited state energies [116, 117, 118, 119, 120, 121]. Recently, the low-lying excited states of ^{12}C have been calculated using non-relativistic lattice methods, including a signature for the Hoyle state [41].

4.2. Scattering parameters

Once the energies of a system have been calculated for a given set of parameters there are many quantities of interest which may then be derived. Scattering parameters form one class of quantities which can be calculated directly from the energy via the Lüscher formula, Eq. (43). According to the Maiani-Testa theorem [122, 123], Euclidean Green's functions cannot give information about infinite volume Minkowski scattering matrix elements except at kinematic thresholds. The Lüscher formula gives an indirect method for calculating these parameters by relating the volume dependence of multi-particle energies to the corresponding infinite volume scattering phase shift. As shown in Fig. 2, the energy eigenvalues for two particles in a periodic box are given by the intercepts of the corresponding $\pi L p \cot\delta$ with the function $\mathcal{S}(\eta)$, defined in Eq. (44).

In [124] it was emphasized that the Lüscher formula is valid for any value of the scattering length, regardless of the size of the box, so that moderately-sized lattices may be used even for scattering processes with unnaturally large scattering lengths. The authors of this work derived approximate expressions giving the explicit volume dependence of the energies of two-body, s-wave scattering states in the limits of small and large scattering length, a/L. In the former limit, the lowest-lying energy is given by

$$E_0 = \frac{4\pi a}{ML^3}\left[1 - c_1\frac{a}{L} + c_2\left(\frac{a}{L}\right)^2 + \cdots\right], \tag{85}$$

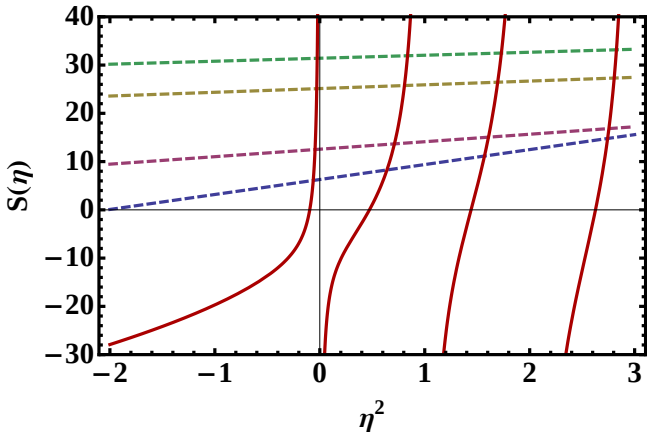

Figure 2. $S(\eta)$ (solid red) and $\pi Lp\cot\delta$ (dashed) vs. $\eta^2 \equiv \left(\frac{pL}{2\pi}\right)^2$. The $\pi Lp\cot\delta$ correspond to the scattering parameters $r_0/a = -0.1$, with the following volumes: $L/|a| = 2$ (blue), $L/|a| = 4$ (magenta), $L/|a| = 8$ (gold), $L/|a| = 10$ (green). The energy eigenstates for the corresponding volumes are given by the intercepts of the curves.

while for the latter one may use

$$E_0 = \frac{4\pi^2}{ML^2}[d_1 + d_2 Lp\cot\delta_0 + \cdots]\,, \tag{86}$$

where c_1, c_2, d_1, d_2 are numerical constants determined in [124], along with analogous expressions for bound states and first excited states. However, in addition to the universal power law dependence of these energies on the size of the box, there exist non-universal exponential corrections due to finite range effects [125, 126], setting a limit on how small the lattice may be for a given scattering process at the desired accuracy.

Generalizations of Eq. (85) to many-body systems have been accomplished using perturbation theory for systems of bosonic particles [127, 128, 129], and successfully applied in lattice QCD calculations of multi-meson states [130, 131, 132, 133, 134]. The Lüscher formula may also be generalized in many other contexts, for example, relations have been derived for asymmetric boxes [135, 136], higher partial waves [137, 138, 139], moving frames [140, 141], moving bound states [142, 143], and multi-channel processes [144, 145].

All of these versions of Lüscher's formula begin with the assumption that the particles exist within a periodic box, a common situation for lattice calculations. In some cases it may be advantageous to consider a different form for the IR cutoff. For example, an adaptation known as the spherical wall method can be useful for determining phase shifts at higher orbital angular momenta, as well as spin-orbit coupling and partial-wave mixing [146]. Here, a hard spherical boundary is imposed in position space, and the eigenvalue problem then becomes one which is well-known from standard nuclear theory texts: the Schrödinger equation is solved given the condition that the wavefunctions must vanish at this spherical boundary. The hard cutoff effectively removes the complications induced by multiple-scattering effects arising from the periodicity of the lattice, however, additional complications arise due to the lack of spherical symmetry on the lattice. This method has proven useful for setting

unknown operator coefficients in lattice chiral EFT methods [37, 38, 39, 40].

Another possibility is to use the eigenvalue solution for two particles in a harmonic potential [147, 148, 149]. Due to progress in the development of nuclear EFT approaches using an oscillator basis [150, 151, 152] and for systems confined in a harmonic potential [153, 154, 155], it has been suggested ([156, 157]) that the spectrum of complex nuclear systems in a harmonic potential may be useful in extracting scattering information using the relation

$$\mathbf{p}^{2l+1}\cot\delta_l(\mathbf{p}) = (-1)^{l+1}(2m\omega)^{l+1/2}\frac{\Gamma\left(\frac{2l+3}{4}-\frac{\epsilon}{2}\right)}{\Gamma\left(\frac{1-2l}{4}-\frac{\epsilon}{2}\right)}, \tag{87}$$

where $\epsilon = E/\omega$. This technique has been demonstrated for two fermions at unitarity [158], and the two nucleon system [157] in the continuum.

It was suggested in [88] that the use of a harmonic potential in lattice calculations may offer some advantages, such as a reduction in noise and fast convergence to the ground state due to the confinement provided by the potential. On the other hand, the potential introduces new physical scales which may induce systematic errors that must be accounted for. For example, because the harmonic potential is non-zero everywhere (except for the origin) there will be modifications to the short range behavior. These finite range effects will not be exponentially suppressed as they are using the standard Lüscher relation, so that an extrapolation to free space ($\omega \to 0$) may be required. Systematic errors associated with harmonic potentials will be discussed in Sec. 6.

4.3. Improved Observables

4.3.1. Energy. The work of Refs. [97, 86] tackles the problem of reducing UV lattice effects by defining an improved the transfer matrix, using a generalized HS transformation and a low-momentum expansion. As we saw at the end of Sec. 2, one may then tune the coefficients C_n such that the two-particle energy spectrum matches the one required by Lüscher's formula for the lowest $N_{\mathcal{O}}$ eigenvalues, given the desired values of the scattering parameters.

The above procedure represents a significant step forward in mitigating lattice-spacing effects in MC calculations, especially considering that it requires only a small coding investment for its implementation in extant MC codes, and it results in minimal computational overhead.

One may use the same technique to eliminate lattice-spacing effects from observables. This is particularly useful in connection with improving finite temperature lattice calculations, such as those of Refs. [109, 25, 159, 160]. Indeed, in those calculations, as well as in similar ground-state approaches, the transfer matrix is not the only object carrying lattice-spacing effects: the operators used to compute expectation values also suffer from the same problems.

The main idea behind the method remains the same as in Ref. [97]. Lüscher's formula provides us with the exact two-particle spectrum, such that the eigenvalues of the exact two-particle transfer matrix and its b_τ derivative(s) are known:

$$-\frac{\partial \mathcal{T}_2^{\text{exact}}}{\partial b_\tau} = E_2 \exp\left(-b_\tau E_2\right) \tag{88}$$

where E_2 are the exact two-particle energies in a continuous box ‡.

‡ We use $\mathcal{T}_2$ here for didactical purposes, but one may use the symmetric expression $\mathcal{T}_2^\dagger\mathcal{T}_2$ instead, with straightforward modifications, as long as this same expression is used in the actual Monte Carlo calculations for a double step in the imaginary-time direction.

Table 2. Results of fitting the coefficients D_n to the low-energy spectrum of the two-body problem at resonance, in a box of side $N_x = 16$, for an imaginary time step $b_\tau = 0.05$, in lattice units.

$N_{\mathcal{O}}$	D_0	D_1	D_2	D_3	D_4
1	-14.76869	–	–	–	–
2	-11.54894	-1.74519	–	–	–
3	-10.74506	-0.96946	-0.40164	–	–
4	-10.31974	-0.82605	-0.17494	-0.10404	–
5	-10.03874	-0.74266	-0.16064	0.02948	-0.02878

In order to match this spectrum, we take the derivative of Eq. (41) with respect to b_τ, evaluated between eigenstates $|E\rangle$ of the proposed transfer matrix $\mathcal{T}_2$. We thus obtain, using the Feynman-Hellmann theorem,

$$-\frac{\partial\langle E|\mathcal{T}_2|E\rangle}{\partial b_\tau} = \langle E|e^{-\frac{b_\tau p_r^2}{2M}}\left[K_2+U_2\right]e^{-\frac{b_\tau q_r^2}{2M}}|E\rangle, \tag{89}$$

where

$$K_2 \equiv \left[\frac{p_r^2}{2M}+\frac{q_r^2}{2M}\right]\left[\delta_{\boldsymbol{p}_r\boldsymbol{q}_r}+\frac{A(\boldsymbol{p}_r)}{2V}\right] \tag{90}$$

and

$$U_2 \equiv -\frac{1}{2V}\frac{\partial A(\boldsymbol{p}_r)}{\partial b_\tau} = \frac{1}{2V}\sum_{n=0}^{N_{max}-1} D_n\mathcal{O}_n(\boldsymbol{p}_r). \tag{91}$$

The rest of the recipe consists in taking the right-hand side of Eq. (89) and fitting the coefficients D_n such that the first $N_{\mathcal{O}}$ eigenvalues of the exact expression Eq. (88) (which correspond to the lowest eigenvalues prescribed by Lüscher's formula) are reproduced. We may assume at this point that the coefficients C_n are known, such that the eigenvectors $|E\rangle$ are fixed when we set out to find the D_n. In that case, the D_n are determined by a linear system of equations of order $N_{\mathcal{O}} \times N_{\mathcal{O}}$:

$$\sum_{n=0}^{N_{\mathcal{O}}-1} M_{En}D_n = Y_E \tag{92}$$

where

$$M_{En} = \frac{1}{2V}\langle E|\mathcal{O}_n|E\rangle \tag{93}$$

and

$$Y_E = E\exp\left(-b_\tau E\right) - \langle E|e^{-\frac{b_\tau p_r^2}{2M}}K_2 e^{-\frac{b_\tau q_r^2}{2M}}|E\rangle \tag{94}$$

Once the coefficients D_n have been determined, one can use this in a lattice calculation simply by replacing $A \to A(\mathbf{p})$, and taking $\partial C_n/\partial b_\tau = D_n$. The results of the fits for D_n are shown in Table 2.

As a first illustration of the level of improvement that can be achieved for the energy, Fig. 3 shows the difference between the approximate spectrum with various levels of improvement E_{approx} and the exact spectrum E_{exact}, as a function of η^2, through the quantity $\log_{10}(|\Delta E|)$, where $\Delta E = (E_{\text{approx}} - E_{\text{exact}})/E_{\text{exact}}$. As expected, with each new parameter a new eigenvalue is reproduced, with the concomitant reduction in the error.

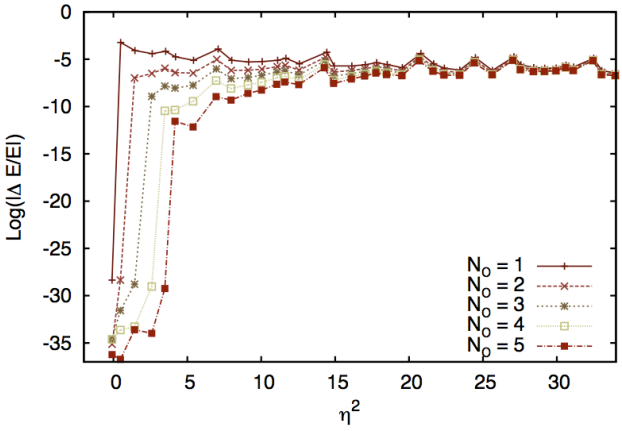

Figure 3. (Color online) Logarithmic plot of the difference between the exact spectrum of the two-body problem Eq. (88) at unitarity, and the approximate spectrum obtained with various levels of improvement $N_{\mathcal{O}} = 1 - 5$, relative to the exact spectrum (see text for details), as a function of $\eta^2 = E_2/p_0^2$, where $p_0 \equiv 2\pi/L$. The original data are discrete; the lines are intended as a guide to the eyes. These results correspond to a lattice of side $N_x = 20$ and temporal spacing $b_\tau = 0.05$.

4.3.2. Contact. The same ideas can be applied to the calculation of Tan's "contact" parameter. One of the many ways to define the contact C (see Refs. [59, 60, 61, 68]) is through the derivative of the energy with respect to the inverse scattering length:

$$\frac{\partial E}{\partial a^{-1}} = -\frac{\hbar^2}{4\pi M} C. \tag{95}$$

The generalization of the above to finite temperature in the grand canonical ensemble is

$$\left(\frac{\partial \Omega}{\partial a^{-1}}\right)_{\beta,\mu} = -\frac{1}{\beta}\left(\frac{\partial \log \mathcal{Z}}{\partial a^{-1}}\right)_{\beta,\mu} = -\frac{\hbar^2}{4\pi M} C(\beta), \tag{96}$$

where Ω is the grand thermodynamic potential, and μ is the chemical potential. In the large-β limit,

$$C(\beta) \underset{\beta\to\infty}{\longrightarrow} C_0 + b_{C1}\beta^{-1} + b_{C2} e^{-\beta\delta} \tag{97}$$

where C_0 is the ground-state contact,

$$b_{C1} = \frac{4\pi M}{\hbar^2}\frac{\partial \log Z_0}{\partial a^{-1}}, \tag{98}$$

$$b_{C2} = -\frac{4\pi M}{\hbar^2}\frac{Z_1}{Z_0}\left(\frac{\partial E_1}{\partial a^{-1}} - \frac{\partial E_0}{\partial a^{-1}}\right). \tag{99}$$

Since E may be obtained directly from the logarithm of the partition function, we are again in a situation where we require a derivative of the transfer matrix with respect to a parameter, in this case a^{-1}.

In many-body lattice calculations, using these definitions involves the following expression:

$$\frac{\partial \mathcal{T}_s[\phi]}{\partial a^{-1}} = e^{-\frac{b_\tau \hat{T}_s}{2}} \hat{U}_{a^{-1}} e^{-\frac{b_\tau \hat{T}_s}{2}} \tag{100}$$

Table 3. Results of fitting the coefficients F_n to the low-energy spectrum of the two-body problem at resonance, in a box of side $N_x = 16$, for an imaginary time step $b_\tau = 0.05$, in lattice units.

$N_{\mathcal{O}}$	F_0	F_1	F_2	F_3	F_4
1	0.36773	–	–	–	–
2	0.14532	0.07568	–	–	–
3	0.11370	0.02220	0.01957	–	–
4	0.09659	0.01695	0.00415	0.00538	–
5	0.08205	0.01278	0.00406	-0.00023	0.00180

where

$$\hat{U}_{a^{-1}} \equiv \frac{\partial\sqrt{A}}{\partial a^{-1}} \sum_{\boldsymbol{i}} \hat{n}_{s,\boldsymbol{i}} \sin\phi_{\boldsymbol{i}}. \tag{101}$$

The first step towards using these expressions in combination with the improvement procedure is to take a formal derivative of $\mathcal{T}$ with respect to a^{-1} in the two-particle space, which we can treat exactly:

$$\frac{d\mathcal{T}_2^{exact}}{da^{-1}} = -b_\tau \frac{\partial E_2}{\partial a^{-1}} \exp\left(-b_\tau E_2\right). \tag{102}$$

In order to compute the change in the exact two-particle energy E_2 due to a small change in the inverse scattering length, we use the fact that the energies are implicitly defined as solutions of Eq. (43), which implies

$$\frac{\partial E_2}{\partial a^{-1}} = -\frac{4\pi^3}{L}\left(\frac{d\mathcal{S}}{d\eta^2}\right)^{-1} \tag{103}$$

where $\eta^2 = E_2 L^2/(2\pi)^2$, and the derivative on the right-hand side is to be evaluated at the corresponding solution of Eq. (43). Table 7 in the Appendix shows the first 30 roots of $S(\eta)$ and the corresponding values of $d\mathcal{S}/d\eta^2$. In the derivation of Eq. (103), we have assumed that all the effective-range parameters other than the scattering length are kept constant.

Having the exact target spectrum, we proceed by finding the corresponding expression in terms of the HS function $A(\mathbf{p})$, which we obtain using Eq. (41) and the Feynman-Hellmann theorem:

$$\frac{\partial\langle E|\mathcal{T}_2|E\rangle}{\partial a^{-1}} = \langle E|e^{-\frac{b_\tau p_r^2}{2M}} \frac{1}{2V} \frac{\partial A(\boldsymbol{p}_r)}{\partial a^{-1}} e^{-\frac{b_\tau q_r^2}{2M}}|E\rangle, \tag{104}$$

where, as before, we expand in terms of our chosen set of operators,

$$\frac{\partial A(\boldsymbol{p}_r)}{\partial a^{-1}} = \sum_{n=0}^{N_{\mathcal{O}}} F_n \mathcal{O}_n(\boldsymbol{p}_r), \tag{105}$$

and we determine the coefficients F_n by fitting the diagonal matrix elements in the right-hand side of Eq. (104) to the exact spectrum of Eqs. (102) and (103). As with the energy, the fitting procedure can be reduced to solving a set of linear equations of order $N_{\mathcal{O}} \times N_{\mathcal{O}}$. Illustrative results of such a fit are shown in Table 3.

As with the energy, a first glimpse at the level of improvement that can be obtained at this point. This is shown in Fig. 4, where we display the difference ΔC

between the spectrum with various levels of improvement and the exact spectrum, divided by the latter. As in Fig. 3, each new parameter allows one to fit a new eigenvalue to high accuracy, matching the desired physics beyond the lowest momentum.

Unlike in Fig. 3, the improvement for eigenvalues beyond those explicitly fit is limited, breaking down after the eighth or ninth eigenvalue. From that point on toward higher energies, little improvement, if any, is observed as the order of the expansion is increased. This behavior is only unexpected in the light of Fig. 3, where the situation is (surprisingly) much more favorable.

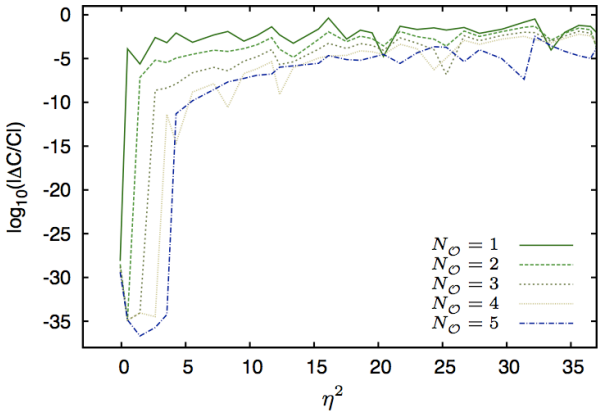

Figure 4. (Color online) Logarithmic plot of the difference between the exact two-body spectrum Eq. (102) at unitarity, and the spectrum obtained with various levels of improvement $N_{\mathcal{O}} = 1 - 5$, relative to the exact spectrum (see text for details), as a function of $\eta^2 = E_2/p_0^2$, where $p_0 \equiv 2\pi/L$. The original data are discrete; the lines are intended as a guide to the eyes. These results correspond to a lattice of side $N_x = 16$ and temporal spacing $b_\tau = 0.05$.

5. Extracting the ground state

5.1. Signal-to-noise

Nonrelativistic systems offer an advantage over relativistic systems concerning the large Euclidean time limit: because there exist no backward propagating states, the entire time extent may be used to recover the ground state. However, there remains a serious issue when taking the large Euclidean time limit that goes beyond the simple linear algorithmic scaling with β. This issue will be referred to as the signal-to-noise problem.

In general, one finds that signal-to-noise problems occur for theories which have multiparticle states for which the energy per particle is lower than for the states one is trying to study. As an example, let us consider a correlation function for a single particle in a two-flavor theory with an attractive interaction between different flavors, a trivial example for which Monte Carlo calculation is not necessary, but which nevertheless illustrates the signal-to-noise problem quite clearly. To determine how many configurations are necessary to achieve a desired accuracy, it is useful to study the signal-to-noise ratio (SNR) as a function of time. To do so, we will follow the prescription of Lepage for determining the SNR for nucleon correlators in Lattice QCD calculations [161]. The signal is given by

$$\begin{aligned} \mathcal{C}_1(\beta) &= \langle K_1(\phi,\beta)\rangle \\ &= \frac{1}{\mathcal{Z}}\int \mathcal{D}\phi \mathcal{P}[\phi] K_1(\phi,\beta), \end{aligned} \tag{106}$$

where

$$K_1(\beta) = \langle 1|B_\beta \cdots B_2 B_1|1\rangle \tag{107}$$

and $|1\rangle$ is a single particle state of interest. As shown in Sec. 4, the correlator is dominated by the ground state at large Euclidean time,

$$\langle K_1(\phi,\beta)\rangle \underset{\beta\to\infty}{\longrightarrow} Z_0^{(1)} e^{-\beta E_0^{(1)}}, \tag{108}$$

where $Z_0^{(n)}, E_0^{(n)}$ are, respectively, the operator overlap with and energy of the ground-state of the n-particle system. For a single particle, we simply have $E_0^{(1)} = 0$, such that at large times the correlator will approach a constant.

Assuming that our sample size is sufficiently large that the central limit theorem holds, the noise may be estimated by calculating the standard deviation,

$$\begin{aligned} \sigma_C^2(\beta) &= \left(\langle |K_1(\phi,\beta)|^2\rangle - |\langle K_1(\phi,\beta)\rangle|^2\right) \\ &= \left(\frac{1}{\mathcal{Z}}\int \mathcal{D}\phi\mathcal{P}[\phi]|K_1(\phi,\beta)|^2 - |\mathcal{C}_1(\beta)|^2\right). \end{aligned} \tag{109}$$

The first term in Eq. (109) is the ensemble average of a product of two single-particle propagators. This may be recognized as a correlator for two degenerate, distinguishable particles. At large Euclidean time, this quantity will be dominated by the ground-state of the two-particle system,

$$\langle |K_1(\phi,\beta)|^2\rangle \underset{\beta\to\infty}{\longrightarrow} Z_0^{(2)} e^{-\beta E_0^{(2)}}. \tag{110}$$

At zero temperature, two particles in a box with an attractive interaction will form a bound state. This means that $E_0^{(2)} < 0$, and the first term in Eq. (109) grows exponentially with time. The second term in Eq. (109) is simply the square of

Eq. (106), which is time-independent. Thus, in the large-β limit it is the first term which dominates.

We can now form the SNR as

$$\mathcal{R} = \frac{\mathcal{C}_1(\beta)}{\sqrt{\frac{1}{N_{\text{cfg}}}\sigma_C^2(\beta)}} \underset{\beta\to\infty}{\longrightarrow} \sqrt{N_{\text{cfg}}}\frac{Z_0^{(1)}}{\sqrt{Z_0^{(2)}}}e^{\beta/2E_0^{(2)}}, \tag{111}$$

Because $E_0^{(2)} < 0$, the SNR is exponentially suppressed as a function of Euclidean time. Thus, an exponentially large number of configurations will be necessary to see a signal at the large times required to extract the ground state from the correlator. An example of an effective mass plot displaying a signal-to-noise problem is illustrated in Fig. 5.1 (left panel).

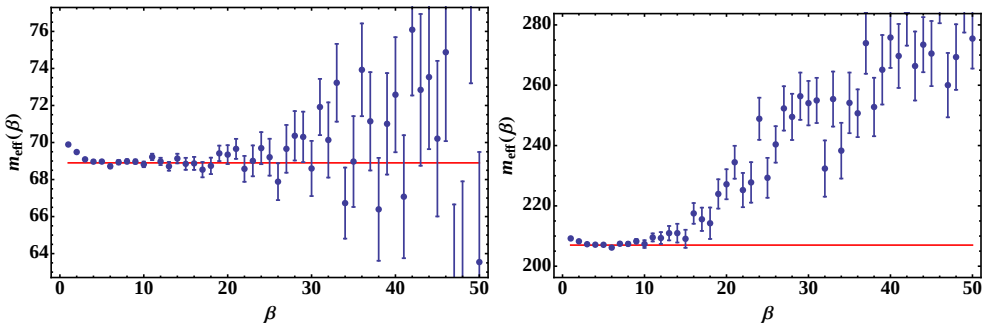

Figure 5. Effective mass plots displaying two common statistical issues: signal-to-noise problem (left), and overlap problem (right). The signal-to-noise problem is seen as an exponential growth of error bars with Euclidean time, while an overlap problem is seen as a drift with no plateau at large Euclidean time. In both cases the ground-state energy is shown as a red line.

One possibility for reducing the signal-to-noise problem lies in the time-independent prefactor in Eq. (111). The overlap factors $Z_0^{(n)}$ depend on how well we are able to model the ground-state wavefunction for our source. Thus, the ability to create sources which have large overlap with the ground state of the observable of interest and poor overlap with the ground state of the system corresponding to the variance may greatly increase the number of time steps over which a signal can be extracted. This has been documented for the case of nucleon correlators in QCD and gives rise to a "golden window" in Euclidean time in which the nucleon is in its ground state but exponential degradation of the signal has not yet set in [162, 163, 164]. In many cases the prefactor is naturally large, for example, in the case of two-component unitary fermions the signal corresponds to a scattering state, while the noise is associated with deeply bound states [165, 166]. The natural choice for a source will correspond to a scattering state and thus $Z_0^{(2)}$, which measures the overlap of the scattering state source with the bound states in the variance, will be much less than 1.

Note that this argument assumes that the central limit theorem holds so that we may identify the noise as coming from the standard deviation of the operator. For many-body operators, this assumption may not in practice be true. Because higher-order moments are sensitive to the energies of higher N-body bound states, it is possible for these moments to also grow exponentially with time. For example,

the third moment of the probability distribution for the single-particle case discussed above will be controlled by the energy of the corresponding three-body state§. Thus, if $E_0^{(3)} \geq 3/2E_0^{(2)}$, the distribution will have non-zero skew which grows exponentially with time. According to the Berry-Esseen theorem [167, 168], the number of configurations necessary for the central limit theorem to apply at a given Euclidean time becomes, $N_{\rm cfg} \gg e^{\beta(2E_0^{(3)}-3E_0^{(2)})}$.

The interpretation of such an issue is that the chosen field distribution is not peaked for configurations on which the operator is peaked. We will refer to this issue as a *distribution* overlap problem. This problem is particularly worrisome because the naïve mean that one calculates may differ significantly from the true quantity, though the error bars may be deceptively small (see Fig. 5.1, right panel). Such a problem will manifest itself in error bars which do not scale with $\sqrt{N_{\rm cfg}}$, and in mean values which drift outside the error bars as the sample size is changed.

The traditional approach to solving this problem is to invoke importance sampling, in which the statistical overlap of $\mathcal{P}[\phi]$ with the desired correlation function is increased by using the correlation function itself in a reweighting procedure. For example, one may work directly with the ratio used for the effective mass, Eq. 81, and rewrite it in the following way:

$$\frac{\mathcal{C}_N(\beta+\Delta\beta)}{\mathcal{C}_N(\beta)} = \frac{\int \mathcal{D}\phi\tilde{\mathcal{P}}[\phi]\mathcal{O}(\phi,\beta)}{\int \mathcal{D}\phi\tilde{\mathcal{P}}[\phi]}\,, \tag{112}$$

where

$$\begin{aligned}\mathcal{O}(\phi,\beta) &= \frac{\tilde{\mathcal{C}}_N(\phi,\beta+\Delta\beta)}{\tilde{\mathcal{C}}_N(\phi,\beta)}\,,\\ \tilde{\mathcal{P}}[\phi] \quad &= \mathcal{P}[\phi]\tilde{\mathcal{C}}_N(\phi,\beta)\,.\end{aligned} \tag{113}$$

The r.h.s. of this equation may be directly sampled using a Monte Carlo algorithm of one's choice according to the new probability measure $\tilde{\mathcal{P}}$, using the observable $\tilde{\mathcal{C}}$. Note that the probability measure is operator-dependent, thus new configurations must be generated for each new type of operator one wishes to study. Despite the added computational cost and complexity of implementing importance sampling, this technique has been used quite successfully in a variety of calculations [90].

An alternative to reweighting is to use a better estimator for $\mathcal{C}(\beta)$ that is free of the distribution overlap problem. One such solution is to use the so-called cumulant expansion for the energy, which relies on the observation that the distribution of the logarithm of the correlator is nearly normally distributed [113]. Such distributions have been shown to be ubiquitous in lattice calculations due to the fact that the correlator consists of many products of matrices of random numbers [113, 165, 169], so that for large N, β the distribution becomes very similar in feature to a log-normal distribution. Furthermore, the log-normal distribution has been shown to be related to systems in which an Efimov effect occurs for distinguishable particles, such as systems of unitary fermions [166].

§ Due to the lack of (anti-)symmetrization between the fields, the three-body state corresponding to the third moment will be composed of particles having three different flavors, with an attractive interaction between all particles. In general, the partition function may correspond to a different number of flavors from the observable; this is referred to in the lattice QCD literature as a "partially quenched" theory.

One may expand the average of a generic correlator

$$\ln\langle C(\beta,\phi)\rangle = \sum_{n=0}^{\infty} \frac{\kappa_n(\beta)}{n!}\,, \tag{114}$$

where κ_n is defined as the n-th cumulant of the distribution for $\ln C(\beta,\phi)$. This may be recognized as the cumulant generating function evaluated at unity. Note that this expansion does not place any assumptions on the particular form of the distribution other than that the expansion exists. However, in general an infinite number of cumulants need to be included for the equality to hold.

On the other hand, if $\ln C(\beta,\phi)$ is nearly normally distributed, all cumulants higher than κ_2 will be small and the series may be truncated at a finite order, n_{max}. Thus the problem has been translated from directly estimating the mean of a quantity having a long-tailed distribution, which is exponentially difficult according to the Berry-Esseen theorem, to that of estimating small moments of a nearly Gaussian distribution. Care must be taken, however, in choosing the order of truncation, and any systematic errors that arise due to truncation must be estimated. An example of results obtained using the cumulant expansion, including evidence for convergence of the series, is shown in Fig. 5.1.

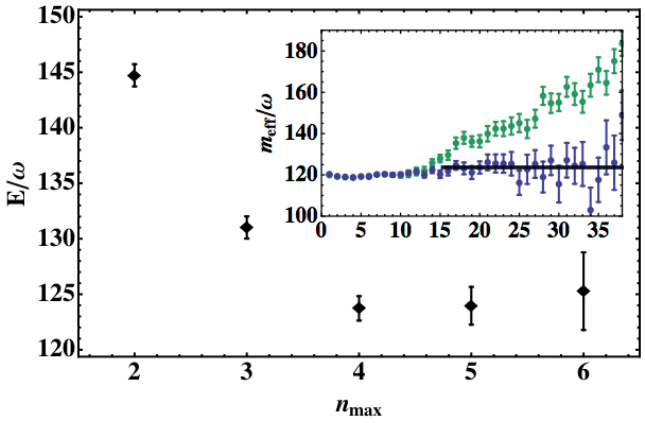

Figure 6. Energy for 50 unitary fermions in a harmonic trap of frequency ω, 10^6 configurations; fits performed using the cumulant expansion (Eq. (114)) truncated at order n_{max}. Inset: conventional effective mass $m_{\rm eff}(\tau) = \log \mathcal{C}(\beta)/\mathcal{C}(\beta+1)$ (green) and corresponding fitted cumulant effective mass with $n_{max} = 4$ (blue). Figure from [165].

5.2. Interpolating fields

The requirement for eliminating excited-state contributions may be approximated as

$$\beta \gg \frac{\ln\left(\frac{Z_1}{E_0 Z_0}\right)}{E_1 - E_0}\,. \tag{115}$$

For many-body systems, the spacing between energy levels may become arbitrarily small as both collective effects and single quasi-particle excitations require relatively small energy to excite. Thus, the number of time steps required to reach the ground state may become quite large for $N \gg 1$. Adding to the complication is the fact

that larger systems tend to probe higher energies than small systems, so that a very fine temporal lattice spacing is required to reduce discretization errors. Finally, the exponentially growing signal-to-noise problem previously discussed may severely limit the time extents for which a signal may be obtained.

To remedy this situation, one may construct improved interpolating fields to try to maximize the overlap with the ground state. For large systems, the ground-state wavefunction becomes increasingly complicated and difficult to parametrize, potentially leading to exponentially poor overlap with a chosen interpolating field as a function of the number of particles. To illustrate this point, we consider the simplest choice for an interpolating field, which is simply a Slater determinant of non-interacting single-particle states. Suppose the ground state of the system consists of non-interacting two-body states. If the overlap of the two-body ground state with the corresponding two-body Slater determinant is ϵ, then the overlap of the N-body state with the N-body Slater determinant will be ϵ^N, giving exponentially poor overlap with the true ground state.

Two-particle correlations may be built in using an $N/2$-body Slater determinant of two-body ground states. For the unitary case, the two-body wavefunction is known and we may build two-particle correlations using this wavefunction. One possibility is to use correlators of the form

$$C_{N_\downarrow,N_\uparrow}(\tau) = \langle \det S^{\downarrow\uparrow}(\tau) \rangle \ , \tag{116}$$

where

$$S^{\downarrow\uparrow}_{i,j}(\tau) = \langle \Psi | K^{-1}(\tau,0) \otimes K^{-1}(\tau,0) | \alpha^\downarrow_i \alpha^\uparrow_j \rangle \ , \tag{117}$$

$|\Psi\rangle$ is the two-body ground state, and $|\alpha^\downarrow \alpha^\uparrow\rangle = |\alpha^\downarrow\rangle \otimes |\alpha^\uparrow\rangle$ are the non-interacting single-particle states. This form of the Slater determinant, in which the pairing correlations are built into the source and not the sink, can be chosen to avoid the order-V increase in computation time required to fully anti-symmetrize both the source and sink. It has been shown [170, 87] that such a form for the correlation functions greatly improves the overlap for systems of unitary fermions. For large, fully interacting systems, 3- and higher-body correlations will also contribute to the ground-state. These may also be built into the interpolating field, however, each of these will increase the computational scaling with V.

Another way to increase the overlap of the interpolating field onto the ground-state wavefunction for systems which possess rotational invariance in the continuum is to project the field onto the appropriate irreducible representation of the cubic group. By doing so, one may eliminate contributions from low-lying excited states with different angular momenta. However, because rotational invariance is broken by the cubic lattice, different angular momentum states can mix. For example, if the ground state of interest has positive parity and zero total angular momentum, one may project onto the A_1^+ representation, which will give overlap with not only the $J = 0$ state, but also $J = 4, 6, \ldots$. Appropriate combinations of sources projected onto different representations may be formed to further eliminate contributions from undesired angular momenta. For details on creating projection operators see App. 9.

6. Systematic effects

In addition to the statistical errors discussed in the previous section, systematic errors arise from the discretization of space and time, as well as from the finite volume of space considered. Furthermore, there may be excited state contributions arising from the finite temporal extent. In this section, we will largely focus on errors due to spatial effects. Temporal discretization errors are subleading to spatial discretization errors, $b_\tau = b_s^2/M$, and may be decreased by increasing the anisotropy parameter M. In addition, as discussed below we may improve the transfer matrix to systematically remove discretization effects. Temporal discretization effects are also reduced by this procedure as the transfer matrix becomes increasingly "perfect" (see Fig. 7). Finally, regarding the issue of finite temporal extent, many improvements to the fitting process have been introduced in the lattice QCD literature, such as multi-exponential fits and removing excited states by calculating correlation functions using multiple sets of sources/sinks [116, 117, 118, 162, 163, 164]. In general, so long as Eq. (115) holds, we may be confident that these effects are exponentially suppressed.

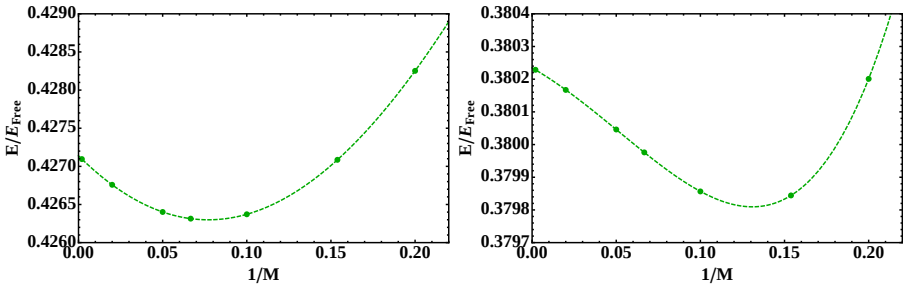

Figure 7. Ground state energy of $N = 2 + 1$ unitary fermions in units of $E_{\text{free}} = (2\pi/L)^2/M$ in the A_1^+ irrep as a function of $1/M$ for one (left) and four (right) tuned couplings with $L = 8$. Dashed green line corresponds to a fourth order polynomial fit in $1/M$. Figure from [89].

6.1. Unitary fermions

To begin our discussion of systematic effects due to spatial discretization and finite volume, we will consider the system of two-component unitary fermions. The lack of physical scales in this system greatly simplifies the analysis. For a review of the introduction of new scales via lattice effective field theory see Ref. [77].

Recall that the relevant scale for this case is the Fermi momentum, $k_F = (3\pi^2 n)^{1/3}$, where $n = N/L_{phys}^3$ is the density. Thus, for a given number of particles the size of the box, $L_{phys} = b_s L$, should be considered a fixed physical scale, and the lattice spacing, or number of lattice points L, will control spatial discretization errors. To reach the continuum limit we require $L \gg 1/(b_s k_F)$.

Finite volume errors of the form a/L may be eliminated by tuning the scattering length according to the Lüscher formalism, which relates the energy levels of two particles in a finite box to the desired scattering phase shift. Note that the Lüscher formalism requires $L \gg r_0/b_s$. As discussed below, a lattice theory will intrinsically induce $r_0 \sim b_s$, placing some constraint on the volumes which may be considered. However, corrections to the Lüscher method due to finite range are exponentially

suppressed, while the non-zero effective range also induces errors which obey power-law behavior to the energies of unitary fermions, so that in general these corrections may be ignored. Finally, we will not discuss the issue of finite size effects in the approach to the thermodynamic limit as these are not particular to the discussion of lattice methods.

Discretization errors arise from two sources. The first is due to the discretization of the kinetic operator. As discussed in Sec. 2, one may improve this discretization by attempting to reproduce the correct single-particle dispersion relation, either by adding higher-order derivative terms and matching the energies order-by-order, or by calculating the kinetic operator directly in momentum space, allowing one to reproduce the exact continuum dispersion relation to all orders up to a momentum cutoff.

The second source of discretization errors comes from the finite range of the interaction induced by the finite lattice spacing. These types of errors may be reduced by improving the two-particle sector. One method for doing so is to introduce momentum-dependent interactions tuned according to Lüscher's formula, as discussed at the end of Sec. 2.

By tuning higher-order energy levels in the two-body spectrum one is also effectively tuning higher-order terms in the effective range expansion of $p \cot \delta$ to zero. This can be verified by plugging the resulting lattice energy eigenvalues back into Lüscher's formula to recover the effective $p \cot \delta$ seen by the two-particle system. This is shown in Fig. 1, where for higher numbers of tuned coefficients $p \cot \delta$ becomes progressively closer to zero for all momenta.

Another way to verify this is by looking at the L-dependence of the energy levels not tuned to the continuum values [97]. The expected scaling of these levels, assuming the leading term in the effective range expansion has been tuned to

$$\pi p/b_s \cot \delta \sim \pi 1/b_s r_{n-1} p^{2n} = \frac{1}{2}(2\pi)^{2n+1} b_s^{2n-1} r_{n-1} \eta^n \,, \tag{118}$$

can be shown to be

$$L\left(\frac{\eta_k}{\eta_k^*} - 1\right) \propto L^{2-2n} \,, \tag{119}$$

where η_k, η_k^* are the kth energy eigenvalue on the lattice and in the continuum respectively. This scaling is confirmed in Fig. 8, which shows the L-dependence of the untuned levels η_5 and η_9.

While reducing the effects of unwanted s-wave scattering contributions, the introduction of momentum-dependent couplings also induces interactions corresponding to higher partial waves. The size of the effects of interactions with angular momenta $\ell > 0$ may be deduced by studying the energies of the two-body lattice eigenstates classified by their irreducible representation (irrep) under the octahedral group O (see Appendix I). Figure 9 shows the deviation of these energy levels $\eta/\eta^* - 1$, where again η, η^* are the energy eigenvalues on the lattice and in the continuum respectively, as a function of η for the entire spectrum for unitary fermions on an $L = 8, 16$ lattice with $N_{\mathcal{O}} = 2, 4$.

Using the generalization of Lüscher's formula for s-wave scattering, we may also determine the scattering phase shifts for the higher partial waves. For p-wave scattering, if one assumes $\tan \delta_4 \ll \tan \delta_1$, one finds (see, for example, [137]):

$$p^3 \cot \delta_1(p) = \left(\frac{2\pi}{L}\right)^3 \frac{1}{2\pi^2}\, \eta\, S(\eta) \,, \tag{120}$$

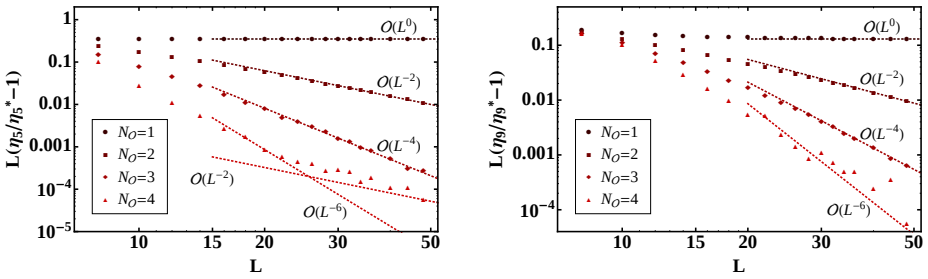

Figure 8. L-dependence of energy eigenvalues for two particles in a box after tuning $N_{\mathcal{O}}$ parameters. Agreement with Eq. 119 for the L-dependence of levels η_5 and η_9 (which were not tuned) shows successful tuning of effective range parameters. Figure from [97].

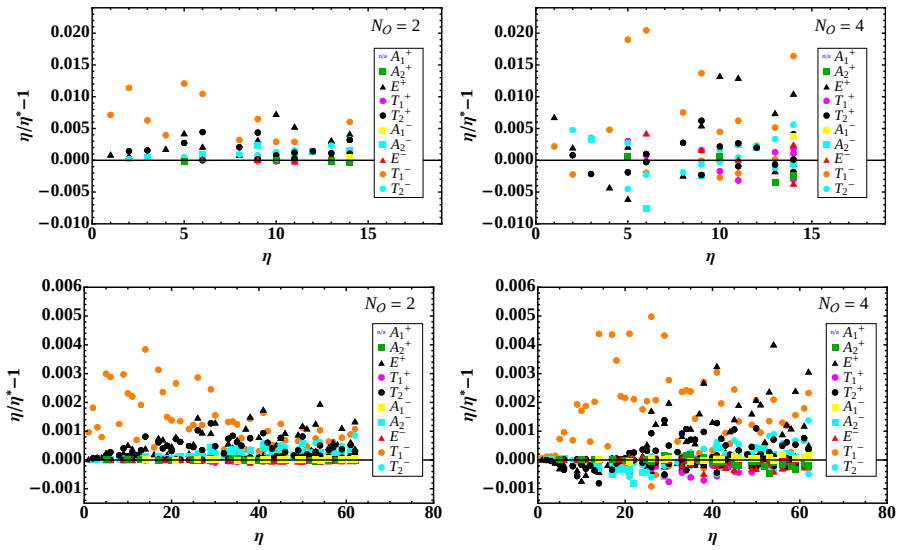

Figure 9. (Color online) Energy spectrum, given by $-\log\lambda = \frac{1}{M}\left(\frac{2\pi}{L}\right)^2\eta$, of two unitary fermions of mass $M = 5$ for two and four tuned couplings in a finite box of size $L = 8, 16$ (top and bottom, respectively); η^* are the corresponding eigenvalues of the noninteracting theory. Eigenvalues are labeled by dimensionality of the irrep to which they belong: square (A), triangle (E), and circle (T), as well as color coded according to the lowest orbital angular momentum component contained in each irrep: orange ($\ell = 1$), black ($\ell = 2$), cyan ($\ell = 3$), magenta ($\ell = 4$), red ($\ell = 5$), green ($\ell = 6$), and yellow ($\ell = 9$). Plots from [89].

where η and $S(\eta)$ are defined in Eq. 43. Plugging the lattice eigenvalues obtained for the T_1^- irrep shown in Fig. 9 into the right-hand side of Eq. 120, we obtain a lattice prediction for $p^3 \cot\delta_1$. This phase shift is plotted in Fig. 10, as a function of η for $L = 16$, and for $N_{\mathcal{O}} = 1, 2, 3, 4$ and 5.

To determine the size of the errors for the N-body system, we may construct the Symanzik effective action [171, 172, 173, 174, 89]. This is done by considering all possible operators formed using the fields and temporal or spatial derivative operators, multiplied by unknown, dimensionless coefficients and appropriate powers of the lattice

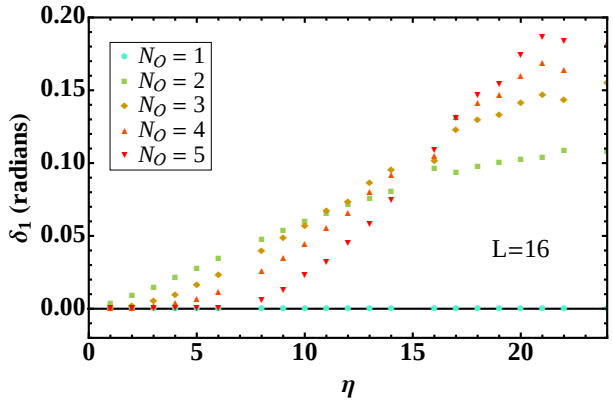

Figure 10. (Color online) δ_1 as a function of the dimensionless parameter η for unitary fermions of mass $M = 5$ on an $L = 16$ lattice obtained from Eq. 120. Figure from [89].

spacings to restore the proper dimension. The first operator to appear, assuming the leading two-body s-wave contributions have been tuned away as discussed above, will be the two-body p-wave interaction discussed above, scaling as L^{-3}. That this scaling behavior dominates in the three-body system is verified in Fig. 14. In principle, one may tune away such p-wave contributions in the same way as the s-wave contributions, by introducing p-wave operators and tuning the coefficients according to the Lüscher formalism.

The next class of operators to appear corresponds to N-body interactions, the lowest being the zero-derivative three-body operator. Such an operator will not obey a naive scaling law due to the conformal nature of the system, but may be shown to scale as $L^{-3.55}$ and $L^{-4.33}$ for $\ell = 1, 0$, respectively, using an operator-state correspondence [175, 52]. Additional operators corresponding to the four-derivative p-wave and d-wave two-body operators come in at order L^{-5}.

Knowledge of the scaling of systematic errors with L are not only useful in estimating the size of systematic errors, but may also be used in an extrapolation to the continuum limit, as seen in Figs. 14,17. For $N = 3$, an extrapolation in $1/L^3$ proved to be sufficient, while higher order contributions were negligible. For $N = 4$ it was found that the contribution from the p-wave three-body operator was non-negligible, so an extrapolation was performed based on the function $c_0 + c_1/L^3 + c_2/L^{3.55}$.

6.2. External potentials

The introduction of an external potential, such as a harmonic trap, may also add new scales to the problem. Furthermore, the way the potential is included in the transfer matrix affects the size of temporal discretization errors. As a simple example, one may use Trotter's product formula in the absence of interactions to eliminate the leading order b_τ contribution,

$$\mathcal{T}_{pot} = e^{-b_\tau K/2} e^{-b_\tau U} e^{-b_\tau K/2} \,. \tag{121}$$

When interactions are turned on, the order at which temporal discretization errors appear depends on how well the interaction has been tuned to remove discretization

errors. If we consider the transfer matrix for unitary fermions without an external potential,

$$\mathcal{T}_{unitary} = e^{-b_\tau K/2} e^{-b_\tau \mathcal{V}_{int}} e^{-b_\tau K/2} \equiv e^{-b_\tau \mathcal{H}}\,, \tag{122}$$

then we may write the full transfer matrix as

$$\mathcal{T} = e^{-b_\tau K/2} e^{-b_\tau U/2} e^{-b_\tau \mathcal{V}_{int}} e^{-b_\tau U/2} e^{-b_\tau K/2}\,. \tag{123}$$

If discretization errors in $\mathcal{H}$ have been completely eliminated by improvement, one may show that temporal discretization errors again come in at $\mathcal{O}(b_\tau^2)$ [97]. The remaining error from temporal discretization may be controlled by tuning the energy scale introduced by the potential of interest; for the case of a harmonic potential, this scale is the trap frequency, ω.

For the simple harmonic oscillator (SHO), a new length scale is introduced, $L_0 = (M\omega)^{1/4}$. Spatial discretization errors are now controlled by the dimensionless ratio L_0/b_s, while finite volume errors are controlled by the independent combination L/L_0.

In the continuum limit, finite volume errors for the noninteracting system may be computed analytically, since the SHO is separable. A plot of the energy dependence of the SHO on L/L_0 is shown in Fig. 11 for several low energy single fermion states; at large L/L_0, the energies in units of ω are just an integer plus the zero point energy (3/2 for a three-dimensional SHO). For very small volumes, the harmonic potential plays no role and the system is effectively a free particle in a finite box, with energies increasing proportional to $\frac{1}{2}\left(\frac{2\pi}{L/L_0}\right)^2$ with decreasing L/L_0. The dashed lines in Fig. 11 indicate this limiting behavior for several SHO states.

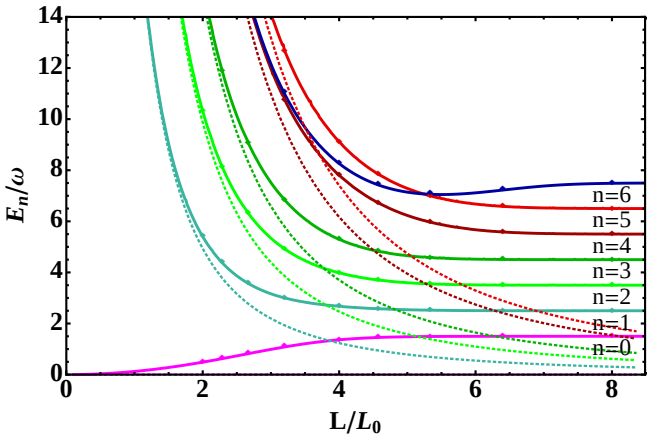

Figure 11. L/L_0 dependence of the SHO energies E_n ($n = \sum_j n_j$) corresponding to the single fermion states $\mathbf{n} = (0,0,0), (1,0,0), (1,1,0), (1,1,1), (2,1,0), (3,1,1)$, and $(4,2,0)$, where $L_0 = (M\omega)^{1/4}$. Solid lines indicate an exact continuum limit calculation, whereas the data-points indicate simulation results for $\omega = 0.005$ and $L_0 \geq 2$. Dotted lines correspond to free fermions in a finite box (small L/L_0 limit). Figure from [97].

When interactions are turned on, in general the errors as a function of L, L_0 must be explored numerically. Benchmark results, which will be presented in the next subsection, are useful in determining values for b_s/L_0 and L/L_0 for which finite

volume and discretization errors are minimal. An example of such a study is shown in Fig. 12.

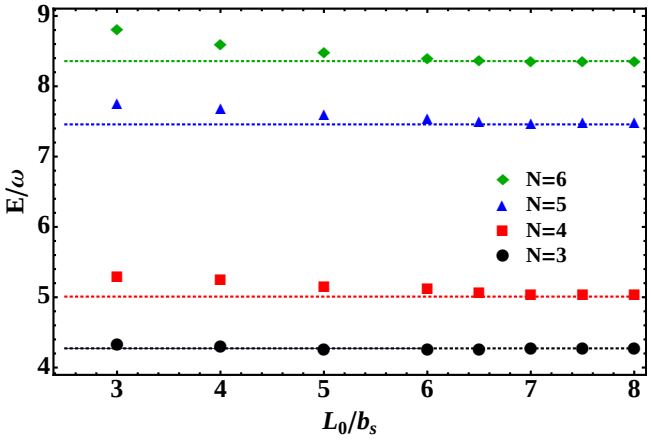

Figure 12. Ground state energies (in units of ω) as a function of L_0/b_s at fixed $L/b_s = 48$ for various values of N, where $L_0 = (M\omega)^{1/4}$. Dotted lines are results from [176]. Figure from [97].

6.3. Comparison with benchmark results

From testing new code to estimating the size of systematic errors for a given parameter set, benchmark results, whether calculated using lattice or other methods such as GFMC, are indispensable when developing new methods. Due to the reduced computational cost and complexity, few-body systems often serve in this role. Such results exist for unitary fermions in both the homogeneous and trapped cases. Verification of these results as the variety of methods grows serves to both strengthen and constrain the results and give validity to new methods.

The simplest system to investigate is that for three unitary fermions in a box. The energies for the first few zero-momentum states were calculated to high accuracy on very large lattices using an unimproved four-fermion interaction in [177], along with a linear extrapolation to the continuum limit (Fig. 13). This measurement was confirmed in [97, 89] using an improved interaction with four tuned coefficients. An extrapolation based on the L^{-3} scaling of the untuned p-wave operators was performed to eliminate the leading contribution to the remaining systematic error (Fig. 14).

Additional benchmarks for three-body observables, the fermion-dimer scattering length and effective range, have been calculated using lattice methods in combination with the Lüscher formalism (see Sec. 4), modified to account for topological corrections to the dimer binding energy [142, 179]. The results found using two different lattice Hamiltonians with a linear extrapolation to the continuum limit are shown in Fig. 15. Also shown is the data computed without correcting for the topological volume factor, $\tau(\eta)$; it is clear that the topological factor has a sizeable impact, particularly on the result for the effective range. Because the scattering amplitude can be reduced to a two-body problem, it can be solved nearly exactly through an integral equation formulation, known as the Skorniakov-Ter-Martirosian (STM) integral equation [180, 181, 182]. Results from the STM equation are included in

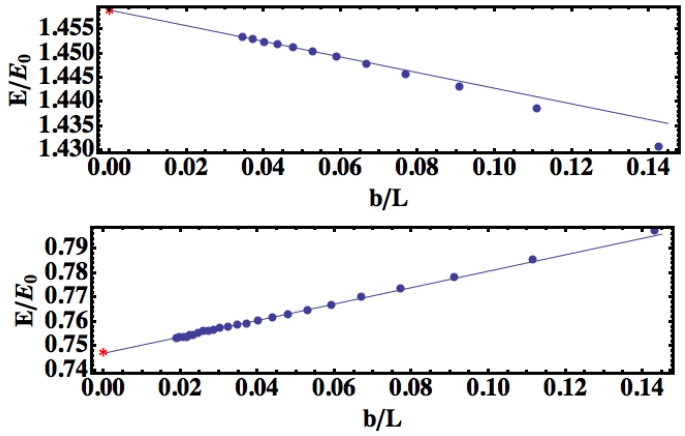

Figure 13. Ground (bottom) and first excited (top) state energies for $N = 2+1$ unitary fermions in a box with zero total angular momentum as a function of b_s/L as calculated in [177]. Energies are in units of $E_0 = 4\pi^2/(2ML^2)$. Lines represent a linear fit to the data for $b_s/L \leq 1/15$, and stars show the energies predicted by the Bethe-Peierls model [178].

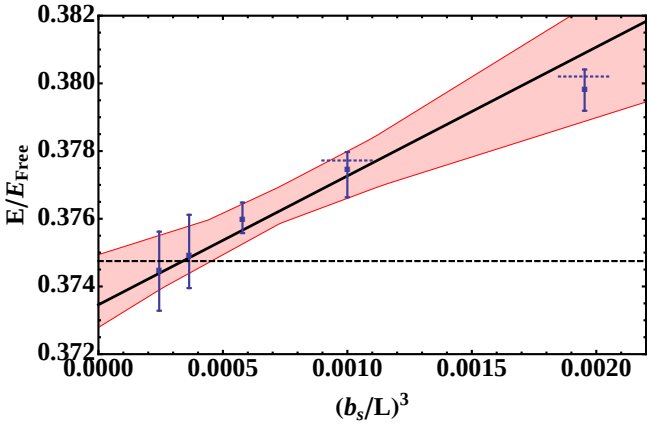

Figure 14. Energy of $N = 2 + 1$ unitary fermions in a zero total momentum eigenstate in units of $E_{\text{free}} = 4\pi^2/(ML^2)$ as a function of $1/L^3$. Blue data points and associated error bars were obtained from numerical simulation, short blue dotted lines at $L = 8$ and $L = 10$ indicate results from exact diagonalization of the three fermion transfer matrix. Red error band indicates the infinite volume extrapolation result reported in [97, 89] using simulation data. Black dashed line indicates the infinite volume result of Pricoupenko and Castin reported in [177]. Figure from [97].

Fig. 15, showing excellent agreement with the lattice results.

The next system to consider is that for four unpolarized unitary fermions in a box. The authors of [183] performed an extensive analysis of this system using four different techniques: hamiltonian lattice formalism using iterated eigenvector methods, Euclidean lattice formalism with auxiliary-field projection Monte Carlo, and continuum diffusion Monte Carlo with fixed and released nodes. The results of polynomial extrapolations to the continuum for the lattice methods are shown in

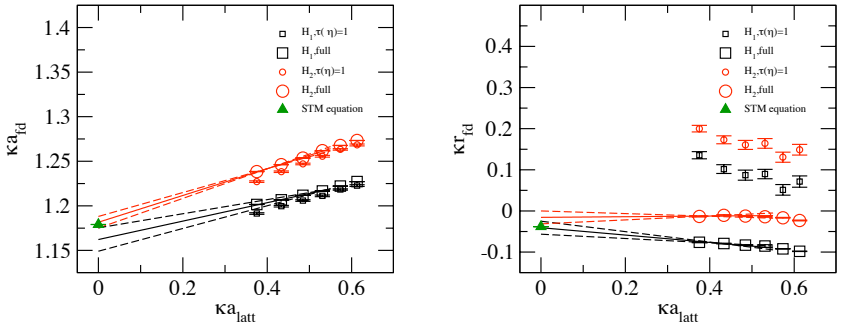

Figure 15. Lattice results and continuum extrapolation with statistical error bands for the fermion- dimer scattering length (left) and effective range (right). All units are given by the binding momentum of the dimer, κ. The full calculation accounts for the topological volume factor, $\tau(\eta) \neq 1$. For comparison the continuum result obtain via the Skorniakov-Ter-Martirosian equation is also presented. Figure from [179].

Fig. 16. The agreement between four different methods gives a very robust benchmark. Additionally, this result was verified in [89] using both an unimproved interaction in conjunction with a linear extrapolation to the continuum limit and an improved interaction with an extrapolation based on the untuned terms in the Symanzik action discussed above (Fig. 17).

Finally, there exist exact results for three unitary fermions in a trap [175, 184], as well as high-precision solutions to the Schrödinger equation for trapped systems of unitary fermions for up to $N = 6$ [185, 176]. These results have been used to tune the parameters L, L_0 for the lattice theory described in [97] (Fig. 12). The final results from the lattice theory have been shown to agree with the benchmark results to within the approximately 1% error bars (see Fig. 18).

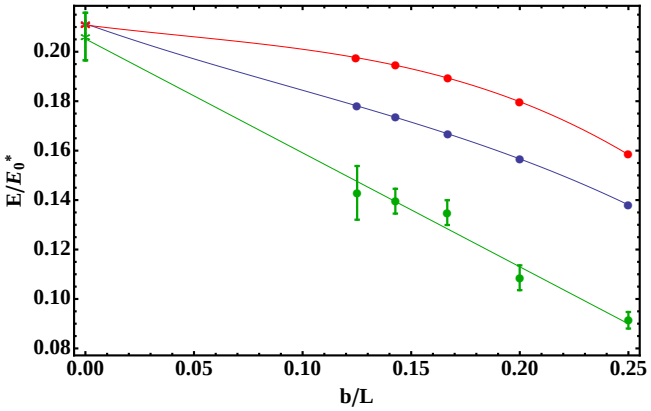

Figure 16. (Color online)Ground state energy for $N = 2+2$ unitary fermions in a box as a function of b/L as calculated in [183] in units of $E_0^* = 4\pi^2/(ML^2)$. The results are extracted using three methods: an exact Hamiltonian lattice method with two different Hamiltonians (blue, red), and a Euclidean lattice method using auxiliary field Monte Carlo (green). Lines represent extrapolations to the infinite volume limit using a third-order polynomial fit (blue, red) and a linear fit (green), with the extrapolated results shown as stars.

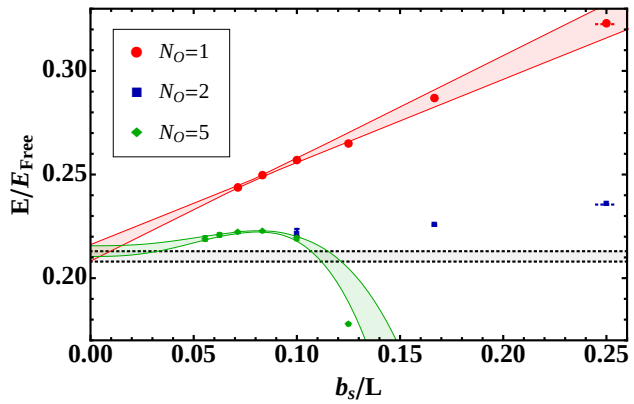

Figure 17. Ground state energy of $N = 2 + 2$ unitary fermions as a function of b_s/L in units of $E_{\rm free} = 4\pi^2/(ML^2)$. Error bars include statistical and fitting systematic errors combined in quadrature. The red and green bands represent fit results to $N_{\mathcal{O}} = 1$ and $N_{\mathcal{O}} = 5$ data as discussed in the text, with error bands reflecting both statistical and systematic errors. Black dotted lines indicate the error band obtained from an infinite volume extrapolation of benchmark calculations reported in [183]. Figure from [89].

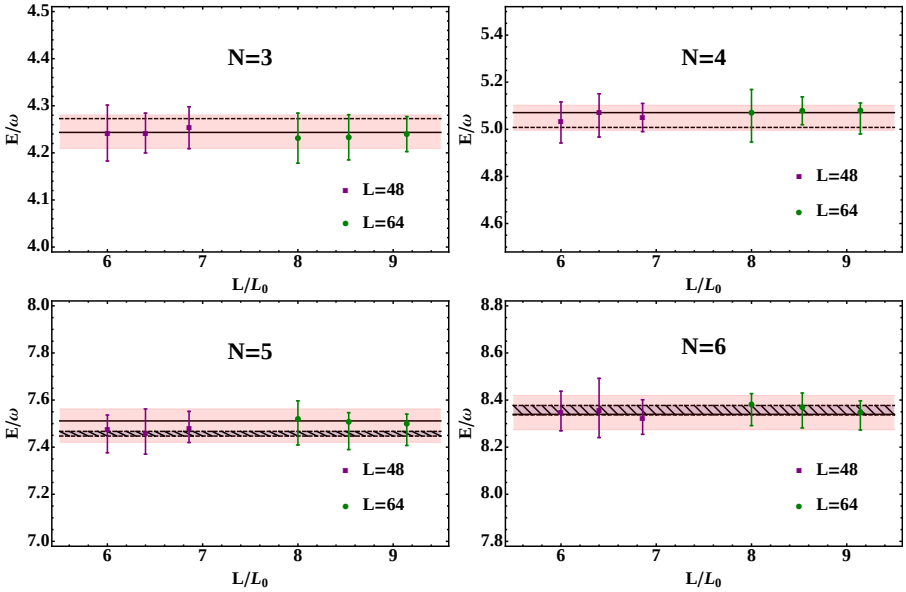

Figure 18. Fit results for the ground state energies (in units of ω) for $N \leq 6$ as a function of L/L_0 for two volumes, $L = 48, 64$, and three trap sizes, $L_0 = 7.0, 7.5, 8.0$. The result of a correlated fit in N, τ of all data is shown as a solid line, with a red band showing the combined statistical and systematic errors. The results from [175, 175] (N=3) and [176] (N=4-6) are given by dashed lines, with any associated error bars shown by hatched regions. Figure from [97].

7. Selected Results

In this section we present a few selected lattice results for few- and many-fermion systems in the unitary limit. This is only a sample of what the methods can accomplish and is by no means fully representative of all the efforts in the field.

7.1. Unitary fermions in a trap

As a first demonstration of the techniques outlined in this article to many-body systems we present results for the ground-state energies of up to $N = 70$ unpolarized unitary fermions in a harmonic trap from [97]. Agreement with benchmark results for this system using an improved action with four tuned couplings were presented in Sec. 6.

In addition to the increased computational time associated with larger systems, many of the issues discussed in previous sections become amplified as the number of particles is increased. For example, as more particles are added to the trapped system, the wavefunction spreads out in coordinate space, increasing sensitivity to the periodic boundary at $x = L$. Therefore, finite volume errors increase and in general one needs to perform an infinite volume extrapolation. To aid in this extrapolation, one may use the knowledge that asymptotically the wavefunction for unitary fermions in a trap has the same behavior as that for free particles in a trap. Thus, finite volume errors will fall off as a Gaussian function, and one may perform a fit of the energies using the following form:

$$f(L/L_0) = E_\infty \left(1 - Ae^{-B(L/L_0)^2}\right) , \tag{124}$$

where E_∞ is the energy at infinite volume, L_0 is the characteristic size of the trap, and A, B are fitting parameters. An example of such an extrapolation is shown in Fig. 19.

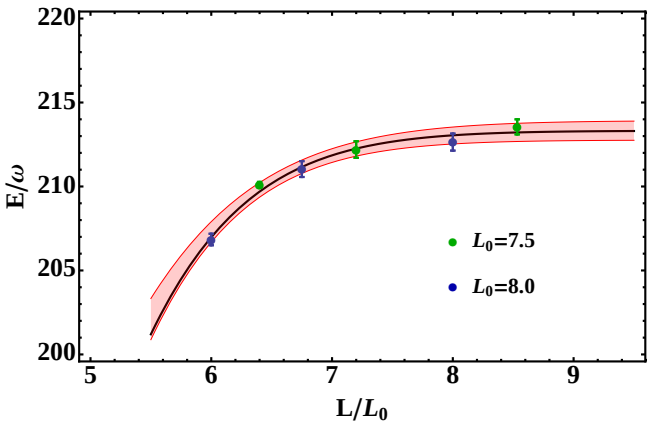

Figure 19. Volume dependence of the ground state energies (in units of ω) for $N = 70$. The data points indicate the individual results for six values of L/L_0, corresponding to two values of $L_0 = 7.5, 8.0$. The infinite volume extrapolation is shown as a solid line, while the band represents the combined statistical and fitting systematic errors from extrapolations performed for the two values of L_0 both separately and combined using Eq. (124). Figure from [97].

The final results for the extrapolated energies as a function of N are shown in Fig. 20 in units of the corresponding energies for N noninteracting fermions in a trap. These results were generated with the same improved action as that for the few-body calculations discussed above using the heat-bath algorithm and utilizing the cumulant expansion Eq. (114) to control the large overlap problem. The combined statistical, fitting systematic, discretization, and finite volume errors are well under the 1% level for large N.

A comparison with two fixed-node calculations, Diffusion Monte Carlo (FN-DMC) and Green's Function Monte Carlo (GFMC), are also shown, along with the benchmark results for $N = 4, 6$. In addition to having generally lower results than the two variational approaches, the lattice data shows marked shell structure, potentially indicating that $N = 70$ is not sufficient to reach the thermodynamic limit for the trapped system.

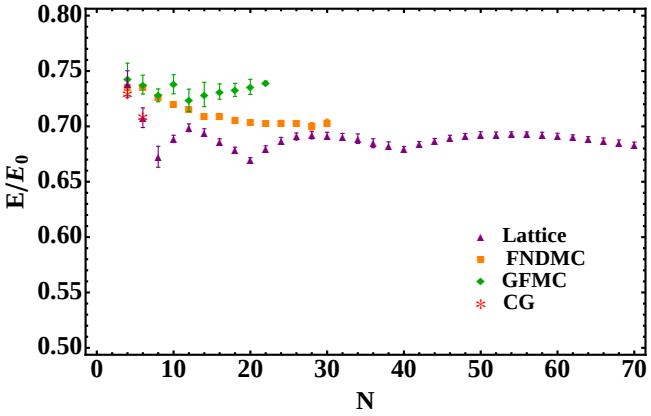

Figure 20. Ground state energies of N trapped unitary fermions in units of the corresponding energies of N trapped noninteracting fermions as a function of N. For comparison, we show results from GFMC [186], FN-DMC [185], and CG [176] methods. Figure from [97].

7.2. Unitary fermions in a box: energy

Lattice results from [89] for the ground-state energies of up to $N = 66$ unpolarized unitary fermions in a periodic box in units of the corresponding noninteracting energies are presented in Fig. 22. As discussed in the Introduction, this ratio of energies is an important universal quantity known as the Bertsch parameter. There have been many calculations of this quantity, both numerical and theoretical, as well as extractions from experiment. A plot of the values reported by various groups is shown in Fig. 21, with values and references for the points in Table 4.

The results presented in Fig. 22 were generated using an improved action with five tuned couplings on lattices ranging from $L = 10 - 14$. The calculation was performed using the heat-bath algorithm in combination with the cumulant expansion to control the overlap problem. The results for this calculation are shown in Fig. 22. The result of a fit to the region $N \geq 34$ (representing the thermodynamic limit) is shown as the last point in Fig. 21.

Due to increased statistical issues, involving both signal-to-noise and overlap

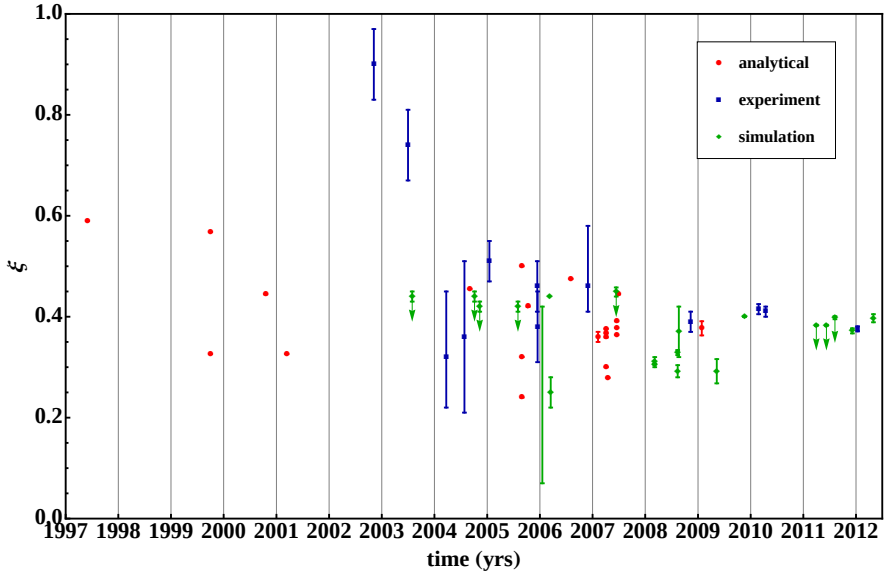

Figure 21. Historical results for the Bertsch parameter determined experimentally, by analytic calculation, and by numerical simulation. Numerical values and citations are tabulated in Table 4. Figure from [89].

problems, with the untrapped system, the error bars for this calculation are larger ($\sim 2\%$) than those for the trapped system, however, they are still competitive with other sophisticated numerical calculations (see Table 4). In addition, the use of a highly improved action shows no variation in the energies with the volume to within the quoted error bars.

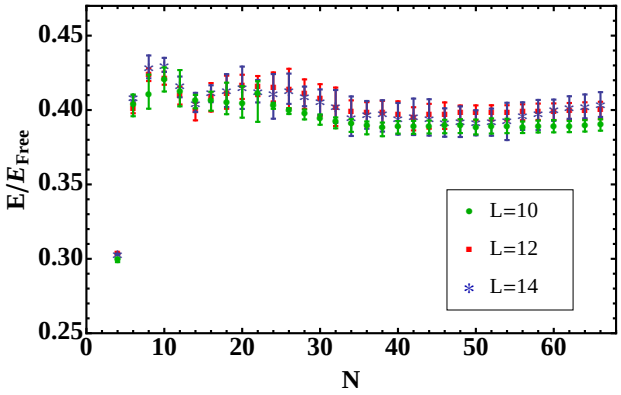

Figure 22. Ground state energy of untrapped unitary fermions in units of $E_{Free}(\rho) = 3NE_F(\rho)/5$, where $E_F(\rho) = (3\pi^2\rho)^{2/3}/2M$, as a function of N for $L = 10, 12$ and $L = 14$. Figure from [89].

Table 4. Historical results for the Bertsch parameter ξ determined experimentally (exp.), by numerical simulation (sim.) and by analytic calculation (anal.), along with publication (pub.) date. Values obtained variationally are upper bounds, and are indicated with an asterisk; simulation results without a quoted error bar should be regarded as approximate.

pub. date	ξ (exp.)	ref.	pub. date	ξ (sim.)	ref.	pub. date	ξ (anal.)	ref.
2002-11-07	0.90(7)	[187]	2003-07-31	0.44(1)*	[170]	1997-06-01	0.59	[188]
2003-07-02	0.74(7)	[189]	2004-10-05	0.44(1)*	[190]	1999-10-01	0.326	[191]
2004-07-27	0.36(15)	[192]	2004-11-10	0.42(1)*	[193]	1999-10-01	0.568	[191]
2004-03-23	0.32^{+13}_{-10}	[194]	2005-08-02	0.42(1)*	[195]	2000-10-19	4/9	[196]
2005-01-16	0.51(4)	[197]	2006-01-18	0.07-0.42	[198]	2001-03-14	0.326	[199]
2005-12-14	0.46(5)	[200]	2006-03-10	0.44	[201]	2004-09-03	0.455	[202]
2005-12-16	0.38(7)	[203]	2006-03-17	0.25(3)	[204]	2005-08-30	0.32	[205]
2006-11-30	0.46^{+12}_{-5}	[206]	2007-06-14	0.449(9)*	[207]	2005-08-30	0.24	[205]
2008-11-11	0.39(2)	[208]	2008-03-07	0.31(1)	[209]	2005-08-30	0.5	[205]
2010-04-15	0.41(1)	[210]	2008-03-07	0.306(1)	[209]	2005-10-11	0.42	[211]
2010-02-25	0.415(10)	[212]	2008-08-13	0.292(12)	[85]	2006-08-04	0.475	[213]
2012-01-12	0.376(4)	[214]	2008-08-13	0.329(5)	[85]	2007-02-08	0.36(1)	[215]
2012-??-??	0.3968(77)	[89]	2008-08-21	0.37 (5)	[25]	2007-04-18	0.279	[216]
			2009-05-11	0.292(24)	[217]	2007-04-05	0.300	[218]
			2009-11-19	0.4	[219]	2007-04-05	0.367	[218]
			2011-04-01	0.383(1)*	[220]	2007-04-05	0.359	[218]
			2011-06-10	0.383(1)*	[221]	2007-04-05	0.376	[218]
			2011-08-08	0.398(3)*	[222]	2007-06-18	0.391	[223]
			2011-12-07	0.372(5)	[90]	2007-06-18	0.364	[223]
						2007-06-18	0.378	[223]
						2007-07-01	4/9	[224]
						2009-01-27	0.377(14)	[225]

7.3. Unitary fermions in a box: contact

To illustrate the effect of improved operators in realistic lattice calculations, this subsection presents the results of ground-state MC calculations of the contact, for an unpolarized system at unitarity.

Results are shown for 80 particles (40 per spin) in a volume of 10^3 lattice points, for various improvement levels $N_{\mathcal{O}} = 1 - 4$. In each case, calculations were performed for time directions of extent $\beta\epsilon_F = 2.0 - 8.0$ (corresponding to N_τ roughly between 40 and 200), subsequently extrapolating to the $\beta \to \infty$ limit. We have taken $b_\tau = 0.05$, and a Slater determinant of plane waves as the starting guess for the ground-state wavefunction. For each value of β, we obtained approximately 400 samples of the auxiliary field ϕ, and the statistics was enhanced by a factor of ~ 20 by inserting operators at every other time slice.

Using extrapolation formulae at leading plus next-to leading order, we obtain $C/(Nk_F) = 3.17(3)$ in the unimproved case, and $C/(Nk_F) = 3.31(4), 3.34(4)$ and $3.30(4)$ for $N_{\mathcal{O}} = 2, 3, 4$, respectively (discarding three data points at the lowest values of $\beta\epsilon_F$ to capture the asymptotic behavior at large β; the fits are stable against further removal of points at low $\beta\epsilon_F$). While the latter extrapolations clearly overlap when taking the uncertainty into account, they do not overlap with the unimproved case, which is clearly consistent with what we see in Fig. 23 at large β. The remaining

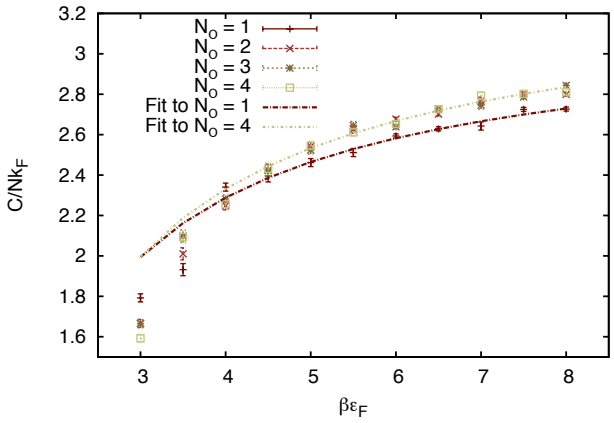

Figure 23. (Color online) Contact, in units of Nk_F, where $k_F = (3\pi^2 N/V)^{1/3}$ is the Fermi momentum, as a function of the extent of the time direction $\beta\epsilon_F = \tau N_\tau \epsilon_F$, for 80 particles and levels of improvement $N_\mathcal{O} = 1 - 4$. Also shown are fits to the $N_\mathcal{O}=1$ and $N_\mathcal{O}=4$ datasets using the first two terms in the asymptotic form of the previous section (see text for details).

systematic errors, likely due to volume effects for the most part, appear to be only as large as 3%, if we consider the most recent estimates of the contact in the ground state (≈ 3.39, see Ref. [220]). Remarkably such a small volume as 10^3 already yields a result that is close to the best current estimate.

8. Summary

In this short review article we have covered some of the most recent progress on the technical aspects of calculating the ground state properties of strongly interacting Fermi gases. We have focused on non-relativistic Hamiltonians with two-body interactions, as relevant for ultracold atom experiments and dilute neutron matter among other systems.

Once the problem is placed on a space-time lattice, the partition function is written as a path integral over the HS auxiliary field. In order to compute expectation values of operators in a non-perturbative fashion, one resorts to stochastic methods to evaluate path integrals, assuming that a useful positive semi-definite probability can be defined. We have discussed various sampling algorithms to accomplish this, from the simplest approaches based on local updates of the auxiliary field, to more sophisticated HMC methods, and a very recent technique based on heat-bath-like ideas.

To reduce lattice-spacing effects one must take the low-density limit and/or implement improved actions, along the lines of similar efforts in Lattice QCD. We have explained how this can be accomplished by designing improved transfer matrices. Furthermore, we have shown that that approach can be extended to the construction of improved operators.

We have also presented a small set of illustrative results.

Finally, the Appendix contains an abridged discussion of some elementary aspects of point group theory, as relevant for the discussion of angular momentum (or its remnants) on the lattice.

Acknowledgments

We gratefully acknowledge discussions with J. Braun, A. Bulgac, J. Carlson, D. Lee, D. B. Kaplan, and M. W. Paris. Part of this work was supported by the U.S. Department of Energy under grants DE-FG02-93ER-40762 and DE-FC02-07ER41457 (UNEDF SciDAC).

9. Appendix I: Group theory on the lattice

9.1. Introduction and basic definitions

When placing a field theory on the lattice, i.e. when replacing the spacetime continuum with a mesh, one obviously loses a fair amount of symmetry. This is the price to pay for going from a problem with infinitely many degrees of freedom to one with a finite number. While we have argued that lower densities and improved actions take us closer to the continuum limit, we have left for this Appendix the more technical discussion of the isometry group associated with the hypercubic lattice.

In order to understand the degree to which the lattice breaks (or preserves) the symmetries of the original theory, it is central to discuss the point group which remains as the unbroken group of rotations, namely the hypercubic group O_h, and its irreducible representations (irreps). Indeed, a subspace of states that transform under a given irrep should remain invariant under time evolution if the original (continuum) Hamiltonian was rotationally invariant. This allows one to classify the scattering states according to the discrete equivalent of angular momentum. As we shall see, there is only a finite number of irreps of O_h, such that the continuum irreps of the rotation group $O(3)$, characterized by an integer l, are decomposed into direct sums of the irreps of O_h.

Following closely the book by Tinkham [226], we shall first review a series of important definitions and theorems (without proof) in the theory of group representations. We will bypass the most elementary definitions concerning the groups themselves.

By definition, a representation of a group is a group consisting of concrete mathematical entities, such as numbers or matrices. In fact, since we are dealing with quantum mechanics, the representations we will discuss are either operators that act on an infinite-dimensional Hilbert space (when speaking about the continuum limit), or actual matrices (when discussing problems on the lattice). We will have in mind the latter case, restricted to square matrices in particular. More specifically, a representation associates a matrix $\mathbf{\Gamma}(A)$ to a given element A of the group in question, such that, given any other element B of the group,

$$\mathbf{\Gamma}(A)\mathbf{\Gamma}(B) = \mathbf{\Gamma}(AB), \tag{125}$$

i.e. the matrices in the representation inherit the multiplication rules from the group. It is easy to convince oneself that, in particular, the identity element E must be mapped onto the identity matrix, i.e. $\mathbf{\Gamma}(E) = \mathbf{E}$. It is also easy to see that from a given representation $\mathbf{\Gamma}$ one can obtain another one $\mathbf{\Gamma}'$ by a similarity transformation on all the matrices: $\mathbf{\Gamma}' = S\mathbf{\Gamma}S^{-1}$. Those two representations are therefore said to be *equivalent*.

In general, representations will be *reducible*, by which we mean that it is possible to bring them to a block-diagonal form by a unitary transformation (one and the same transformation for the whole original representation), or otherwise *irreducible* if this is not possible.

In this context, the following lemma is often useful: *Any representation by matrices with non-vanishing determinant is equivalent through a similarity transformation to a representation in terms of unitary matrices.*

This lemma is useful in particular when proving the famous Schur's lemma: *Any matrix which commutes with all the matrices of an irreducible representation must be a*

multiple of the identity matrix. If such a non-constant matrix exists, the representation must be reducible; if it does not exist, then the representation is irreducible.

9.2. Orthogonality theorems, characters and conjugacy classes

The above are very important, but somewhat formal statements. They allow, however, to prove an identity concerning the orthogonality property of the representations that is extremely useful in practice:

$$\sum_R \mathbf{\Gamma}^{(i)}(R)^*_{\mu\nu}\mathbf{\Gamma}^{(j)}(R)_{\alpha\beta} = \frac{h}{l_i}\delta_{ij}\delta_{\mu\alpha}\delta_{\nu\beta}, \tag{126}$$

where the sum is over all the group elements, i, j denote particular representations, l_i is the dimension of the i-th representation, and h is the order of the group (i.e. the number of elements in it). This equation is valid when i, j denote *irreducible*, *inequivalent*, *unitary* representations of the group in question.

As we shall see, this statement is quite powerful. It can be interpreted geometrically if we set $i = j$ and regard R as denoting a coordinate in a vector space of dimension h. The above is then a statement of orthogonality between as many vectors as matrix elements in the i-th representation, of which there are l_i^2. This is valid for all representations, so the above indicates that there are $\sum_i l_i^2$ orthogonal vectors. But if the dimension of space is h, then we must have $\sum_i l_i^2 \leq h$. As it turns out, the equality is valid, so we have

$$\sum_i l_i^2 = h, \tag{127}$$

which dramatically constrains the possible dimensions of the collection of irreducible, inequivalent, unitary representations of the group.

We may also obtain a statement about the traces $\chi^{(i)}(R) = \mathrm{Tr}\,\mathbf{\Gamma}^{(i)}(R)$ of the matrices in the representation. These are usually referred to as *characters* and they have a special name because they are invariant under similarity transformations, such that they are a specific signature of each representation. Summing over $\mu = \nu$ and $\alpha = \beta$, we see that characters are orthogonal:

$$\sum_R \chi^{(i)}(R)^*\chi^{(j)}(R) = h\delta_{ij}. \tag{128}$$

Within a group it is generally possible to identify subsets of elements which, when taken together, form a partition (i.e. the subsets are such that each element belongs to one and only one subset, and the union of all the subsets yields the full group). Each subset is defined by the following (equivalence) relation: Two elements A and B in the group are said to be *conjugate* to each other if an element X exists such that

$$A = XBX^{-1}. \tag{129}$$

The subsets in the partition are therefore referred to as *conjugacy classes*, and contain elements connected to each other by the above relation. Clearly, the identity element E is in a class by itself, as it cannot be conjugate to any other element. In the context of groups of symmetry transformations, which is the application we have in mind here, conjugacy classes roughly correspond to different kinds of operations (e.g. rotations about a particular axis).

With the above definition, it is clear that the characters of two elements that are in the same class will be the same. We may therefore consider the characters of the classes $\mathcal{C}_k$ within a given representation i instead of those of each of the elements R:

$$\sum_R \chi^{(i)}(R)^* \chi^{(j)}(R) = \sum_k \chi^{(i)}(\mathcal{C}_k)^* \chi^{(j)}(\mathcal{C}_k) N_k = h\delta_{ij}, \tag{130}$$

where N_k is the number of elements in the k-th class. Once again, a geometric interpretation helps: If we regard the characters as vectors with entries in the space of conjugacy classes, then the above indicates that there exist as many orthogonal vectors in this space as irreducible representations. But clearly this number cannot exceed the dimensionality of the space. Therefore, the number of inequivalent, unitary irreps N_{irreps} is less than or equal to the number of classes $N_{\mathcal{C}}$. As it turns out, they are equal:

$$N_{irreps} = N_{\mathcal{C}}. \tag{131}$$

Using the above identities one can also show another orthogonality relation between characters:

$$\sum_i \chi^{(i)}(\mathcal{C}_k)^* \chi^{(i)}(\mathcal{C}_l) = \frac{h}{N_k} \delta_{kl}. \tag{132}$$

9.3. Decomposition of reducible representations

If you were wondering when all of the above would become useful, this is it.

The character of a reducible representation is obviously the sum of the characters of all the representations it contains, i.e.

$$\chi(R) = \sum_j a_j \chi^{(j)}(R) \tag{133}$$

where a_j is the multiplicity of the j-th irrep, i.e. the number of times it appears. The above orthogonality relations can therefore help us identify the irrep content of a given representation:

$$a_j = h^{-1} \sum_R \chi^{(j)}(R)^* \chi(R) = h^{-1} \sum_k N_k \chi^{(j)}(\mathcal{C}_k)^* \chi(\mathcal{C}_k). \tag{134}$$

9.4. Projection operators for irreducible representations

Let the basis of the j-th irrep be denoted by $\varphi_\alpha^{(j)}$, where $\alpha = 1, ..., l_j$. Given a particular basis element $\varphi_\kappa^{(j)}$, the other ones are usually referred to as *partners*. By definition, the action of an element of the group on $\varphi_\kappa^{(j)}$ can be expanded as a linear combination in the basis of that function and its partners:

$$P_R \varphi_\kappa^{(j)} = \sum_{\lambda=1}^{l_j} \varphi_\lambda^{(j)} \mathbf{\Gamma}^{(j)}(R)_{\lambda,\kappa}. \tag{135}$$

Multiplying by $\mathbf{\Gamma}^{(i)}(R)^*_{\lambda',\kappa'}$, summing over R, and using the orthogonality theorems, we obtain

$$\sum_R \mathbf{\Gamma}^{(i)}(R)^*_{\lambda',\kappa'} P_R \varphi_\kappa^{(j)} = \frac{h}{l_j} \delta_{ij} \delta_{\kappa,\kappa'} \varphi_{\lambda'}^{(j)}. \tag{136}$$

Clearly then, applying to a function the operator

$$\mathscr{P}^{(j)}_{\lambda\kappa} = \frac{l_j}{h} \sum_R \mathbf{\Gamma}^{(j)}(R)^*_{\lambda,\kappa} P_R \tag{137}$$

yields zero unless the function has a projection on the κ-th basis element of the j-th representation, in which case the result is transferred onto the λ-th direction. For this reason these operators are sometimes referred to as *transfer* operators. The special case $\lambda = \kappa$ yields a *projection* operator, as in that case we have

$$\mathscr{P}^{(j)}_{\kappa\kappa} \varphi^{(j)}_\kappa = \varphi^{(j)}_\kappa. \tag{138}$$

While the above identities are useful when we already know the explicit form of the Γ matrices, one can still obtain practical results by knowing just the characters. Indeed, setting $\lambda = \kappa$ in Eq. 137 and summing over κ we obtain a new projection operator

$$\mathscr{P}^{(j)} = \sum_\kappa \mathscr{P}^{(j)}_{\kappa\kappa} = \frac{l_j}{h} \sum_R \chi^{(j)}(R)^* P_R \tag{139}$$

which projects onto the j-th irrep.

9.5. The octahedral group

By far the most common choice in lattice field theory calculations is to discretize spacetime as a hypercubic mesh. Therefore the point group one is concerned with is the so-called *octahedral* group O. This group contains the proper (no parity transformations) rotations which take a cube or an octahedron into itself. In this case $h = 24$, i.e. it has 24 elements, which include, apart from the identity (E), eight rotations about cube body diagonals ($8C_3$), nine rotations around the X,Y,Z axes ($3C_2$ plus $6C_4$), and six rotations about axes parallel to face diagonals ($6C_2$). Should we choose to include the inversion operation as well, which form the group i, we will then obtain the group O_h, where $O_h = O \times i$. This is referred to as the *full octahedral* group, and with 48 elements it is the largest of all the point groups.

Table 5. Table of characters of the octahedral group O.

	E	$8C_3$	$3C_2$	$6C_2$	$6C_4$
A_1	1	1	1	1	1
A_2	1	1	1	-1	-1
E	2	-1	2	0	0
T_1	3	0	-1	-1	1
T_2	3	0	-1	1	-1

The table of characters of O is shown in Table 5. The classes appear in the top row, and the irreps along the first column. The dimensionality of each irrep can be read from the second column.

While we have only 5 irreps for O, in the continuum we have $SO(3)$, and therefore an infinite number of irreps, parametrized by an integer ℓ, with dimensions given by $2\ell + 1$ and spanned by the spherical harmonics Y^m_ℓ. It is therefore natural to ask: within each irrep of $SO(3)$, how is the dimensionality split among the finite number of irreps of the octahedral group when we put the problem on the lattice?

In order to answer this question, we may simply use the character orthogonality relations on the ℓ-th representation of $SO(3)$. We need only know the character of the elements of O, now interpreted as elements of $SO(3)$, in that representation, which are given by

$$\chi^{\ell}(\alpha) = \frac{\sin(\ell + \frac{1}{2})\alpha}{\sin(\alpha/2)}. \tag{140}$$

Thus,

$$\chi(C_2) = \chi(\pi) = (-1)^{\ell}$$
$$\chi(C_3) = \chi(2\pi/3) = \begin{cases} 1 & \ell = 0, 3, \ldots \\ 0 & \ell = 1, 4, \ldots \\ 1 & \ell = 2, 5, \ldots \end{cases}$$
$$\chi(C_4) = \chi(\pi/2) = \begin{cases} 1 & \ell = 0, 1, 4, 5, \ldots \\ -1 & \ell = 2, 3, 6, 7, \ldots \end{cases} .$$

Using these results one may then decompose the s-wave, p-wave, etc., representations of $SO(3)$ in terms of the irreps of the octahedral group. The (partial) result of such a decomposition is shown in Table 6. A considerably more thorough treatment of this problem appears in Ref. [137]. From the table we see that only the A_1 representation contributes to s-wave scattering, but it also appears in higher waves. For $\ell > 4$ the various irreps of O will in general appear more than once.

Table 6. Characters and decomposition of irreps of $SO(3)$ into irreps of the octahedral group O.

ℓ	E	$8C_3$	$3C_2$	$6C_2$	$6C_4$	Decomposition
0	1	1	1	1	1	A_1
1	3	0	-1	-1	1	T_1
2	5	-1	1	1	-1	$E + T_2$
3	7	1	-1	-1	-1	$A_2 + T_1 + T_2$
4	9	0	1	1	1	$A_1 + E + T_1 + T_2$

10. Appendix II: Roots and first derivative of $S(\eta)$

Table 7. First 30 roots of $\mathcal{S}(\eta)$, and $d\mathcal{S}/d\eta^2$ evaluated at those roots.

k	η_k^2	$d\mathcal{S}/d\eta_k^2$
1	-0.0959007	123.82387
2	0.4728943	39.75514
3	1.4415913	82.36519
4	2.6270076	106.24712
5	3.5366199	84.23133
6	4.2517060	161.88763
7	5.5377008	212.49220
8	7.1962632	62.95336
9	8.2879537	231.79580
10	9.5345314	247.82611
11	10.5505341	233.82976
12	11.7014957	185.61411
13	12.3102392	183.65019
14	13.3831152	316.68684
15	15.3537375	82.86757
16	16.1218253	506.59914
17	17.5325415	371.40245
18	18.6053932	308.00372
19	19.5186394	255.97969
20	20.4033187	329.98905
21	21.6944179	394.81924
22	23.0194727	94.98929
23	24.3306210	342.25749
24	25.3016129	526.27127
25	26.6803600	514.90705
26	27.8780019	150.20773
27	29.6156511	548.38017
28	31.3536974	114.02114
29	32.1958982	443.21169
30	33.4483351	452.78989

References

[1] A. Lüchow and J. B. Anderson. Monte carlo methods in electronic structures for large systems. *Annu. Rev. Phys. Chem.*, 51:501, 2000.

[2] J. Carlson and R. Schiavilla. Structure and dynamics of few-nucleon systems. *Rev. Mod. Phys.*, 70:743, 1998.

[3] M. H. Kalos and P. A. Whitlock. *Monte Carlo Methods, 2nd ed.* WILEY-VCH Verlag, Weinheim, 2008.

[4] R. J. Bartlett and M. Musial. Coupled-cluster theory in quantum chemistry. *Rev. Mod. Phys.*, 79:291, 2007.

[5] D. J. Dean and M. Hjorth-Jensen. Coupled-cluster approach to nuclear physics. *Phys. Rev. C*, 69:54320, 2004.

[6] P. Navrátil, S. Quaglioni, I. Stetcu, and B. R. Barrett. Recent developments in no-core shell-model calculations. *J. Phys. G*, 36:083101, 2009.

[7] B. S. Pudliner, V. R. Pandharipande, J. Carlson, S. C. Pieper, and R. B. Wiringa. Quantum monte carlo calculations of nuclei with $a \leq 7$. *Phys. Rev. C*, 56:1720, 1997.

[8] R. B. Wiringa, S. C. Pieper, J. Carlson, and V. R. Pandharipande. Quantum monte carlo calculations of $a = 8$ nuclei. *Phys. Rev. C*, 62:014001, 2000.

[9] S. C. Pieper and R. B. Wiringa. Quantum monte carlo calculations of light nuclei. *Ann. Rev. Nucl. Part. Sci.*, 51:53, 2001.

[10] S. C. Pieper, V. R. Pandharipande, R. B. Wiringa, and J. Carlson. Realistic models of pion-exchange three-nucleon interactions. *Phys. Rev. C*, 64:014001, 2001.

[11] S. C. Pieper, K. Varga, and R. B. Wiringa. Quantum monte carlo calculations of $a = 9, 10$ nuclei. *Phys. Rev. C*, 66:044310, 2002.

[12] R. B. Wiringa and S. C. Pieper. Evolution of nuclear spectra with nuclear forces. *Phys. Rev. Lett.*, 89:182501, 2002.

[13] S. C. Pieper, R. B. Wiringa, and J. Carlson. Quantum monte carlo calculations of excited states in $a = 6 - 8$ nuclei. *Phys. Rev. C*, 70:054325, 2004.

[14] G. Hagen, D. J. Dean, M. Hjorth-Jensen, and T. Papenbrock. Complex coupled-cluster approach to an ab-initio description of open quantum systems. *Phys. Lett. B*, 656:169, 2007.

[15] G. Hagen, D. J. Dean, M. Hjorth-Jensen, T. Papenbrock, and A. Schwenk. Benchmark calculations for ^{3}h, ^{4}he, ^{16}o, and ^{40}ca with ab initio coupled-cluster theory. *Phys. Rev. C*, 76:044305, 2007.

[16] G. Hagen, T. Papenbrock, D. J. Dean, A. Schwenk, A. Nogga, M. Włoch, and P. Piecuch. Coupled-cluster theory for three-body hamiltonians. *Phys. Rev. C*, 76:034302, 2007.

[17] G. Hagen, T. Papenbrock, D. J. Dean, and M. Hjorth-Jensen. Medium-mass nuclei from chiral nucleon-nucleon interactions. *Phys. Rev. Lett*, 101:092502, 2008.

[18] P. Navratil, J. P. Vary, and B. R. Barrett. Properties of ^{12}c in the ab initio nuclear shell model. *Phys. Rev. Lett*, 84:5728, 2000.

[19] P. Navratil and W. E. Ormand. Ab initio shell model with a genuine three-nucleon force for the p-shell nuclei. *Phys. Rev. C*, 68:034305, 2003.

[20] E. Caurier and P. Navratil. Proton radii of ^{4,6,8}he isotopes from high-precision nucleon-nucleon interactions. *Phys. Rev. C*, 73:021302(R), 2006.

[21] H. Rothe. *Lattice Gauge Theories, 3rd ed.* World Scientic, Singapore, 2005.

[22] T. DeGrand and C. DeTar. *Lattice Methods for Quantum Chromodynamics.* World Scientic, Singapore, 2006.

[23] A. Bazavov, D. Toussaint, C. Bernard, J. Laiho, C. DeTar, L. Levkova, M. B. Oktay, S. Gottlieb, U. M. Heller, J. E. Hetrick, P. B. Mackenzie, R. Sugar, and R. S. Van de Water. Nonperturbative qcd simulations with $2 + 1$ flavors of improved staggered quarks. *Rev. Mod. Phys.*, 82:1349–1417, May 2010.

[24] R. R. dos Santos. Introduction to quantum monte carlo simulations for fermionic systems. *Braz. J. Phys.*, 36:33, 2003.

[25] A. Bulgac, J.E. Drut, and P. Magierski. Quantum monte carlo simulations of the bcs-bec crossover at finite temperature. *Phys. Rev. A*, 78:023625, 2008.

[26] E.T. Jaynes. *The Maximum Entropy Formalism, edited by R.D. Levine and M. Tribus.* MIT Press, Cambridge, MA, 1978.

[27] M. Jarrell and J.E. Gubernatis. Bayesian inference and the analytic continuation of imaginary-time quantum monte carlo data. *Physics Reports*, 269:133, 1996.

[28] J. E. Drut and T. A. Lähde. Lattice field theory simulations of graphene. *Phys. Rev. B*, 79:165425, 2009.

[29] J. E. Drut and T. A. Lähde. Is graphene in vacuum an insulator? *Phys. Rev. Lett.*, 102:026802, 2009.

[30] J. E. Drut and T. A. Lähde. Critical exponents of the semimetal-insulator transition in graphene: A monte carlo study. *Phys. Rev. B*, 79:241405, 2009.

[31] S. J. Hands and C. G. Strouthos. Quantum critical behavior in a graphenelike model. *Phys. Rev. B*, 78:165423, 2008.

[32] W. Armour, S. Hands, and C. Strouthos. Monte carlo simulation of the semimetal-insulator phase transition in monolayer graphene. *Phys. Rev. B*, 81:125105, 2010.

[33] W. Armour, S. Hands, and C. Strouthos. Monte carlo simulation of monolayer graphene at nonzero temperature. *Phys. Rev. B*, 84:075123, 2011.

[34] R. Brower, C. Rebbi, and D. Schaich. Hybrid monte carlo simulation on the graphene hexagonal lattice. *PoS*, Lattice 2011:056, 2011.

[35] E. Epelbaum, H.-W. Hammer, and U.-G. Meiβner. Modern theory of nuclear forces. *Rev. Mod. Phys.*, 81:1773, 2009.

[36] B. Borasoy, E. Epelbaum, H. Krebs, D. Lee, and U.-G. Meiβner. Lattice simulations for light nuclei: Chiral effective field theory at leading order. *Eur. Phys. J. A*, 31:105, 2007.

[37] B. Borasoy, E. Epelbaum, H. Krebs, D. Lee, and U.-G. Meiβner. Chiral effective field theory on the lattice at next-to-leading order. *Eur. Phys. J. A*, 35:343, 2008.

[38] E. Epelbaum, H. Krebs, D. Lee, and U.-G. Meiβner. Lattice chiral effective field theory with three-body interactions at next-to-next-to-leading order. *Eur. Phys. J. A*, 41:125, 2009.

[39] E. Epelbaum, H. Krebs, D. Lee, and U.-G. Meiβner. Lattice calculations for a=3,4,6,12 nuclei using chiral effective field theory. *Eur. Phys. J. A*, 45:335, 2010.

[40] E. Epelbaum, H. Krebs, D. Lee, and U.-G. Meiβner. Lattice effective field theory calculations for a = 3,4,6,12 nuclei. *Phys. Rev. Lett.*, 104:142501, 2010.

[41] E. Epelbaum, H. Krebs, D. Lee, and U.-G. Meiβner. Ab initio calculation of the hoyle state. *Phys. Rev. Lett.*, 106:192501, 2011.

[42] U.-G. Meiβner. Nuclear physics from simulations. *Few-Body Syst.*, 50:91, 2011.

[43] S. R. Beane, K. Orginos, and M. J. Savage. Hadronic interactions from lattice qcd. *Int. J. Mod. Phys. E*, 17:1157, 2008.

[44] S. R. Beane, W. Detmold, K. Orginos, and M. J. Savage. Nuclear physics from lattice qcd. *Prog. Part. Nucl. Phys.*, 66:1, 2011.

[45] S. Giorgini, L.P. Pitaevskii, and S. Stringari. Theory of ultracold fermi gases. *Rev. Mod. Phys.*, 80:1215, 2008.

[46] I. Block, J. Dalibard, and W. Zwerger. Many-body physics with ultracold gases. *Rev. Mod. Phys.*, 80:885, 2008.

[47] M. Inguscio, W. Ketterle, and C. Salomon. *Ultracold Fermi Gases, Proceedings of the International School of Physics "Enrico Fermi," CourseCLXIV, Varenna, June 20-30.* IOS Press, Amsterdam, 2008.

[48] T. L. Ho. Universal thermodynamics of degenerate quantum gases in the unitarity limit. *Phys. Rev. Lett.*, 92:090402, 2004.

[49] F. Werner and Y. Castin. Springer-Verlag, Berlin, 2011.

[50] E. Braaten and H.-W. Hammer. Universality in few-body systems with large scattering length. *Phys. Rept.*, 428:259, 2006.

[51] T. Mehen, I. W. Stewart, and M. B. Wise. Conformal invariance for non-relativistic field theory. *Phys. Lett. B*, 474:145, 2000.

[52] Y. Nishida and D. T. Son. Nonrelativistic conformal field theories. *Phys. Rev. D*, 76:086004, 2007.

[53] C. R. Hagen. Scale and conformal transformations in galilean-covariant field theory. *Phys. Rev. D*, 5:377, 1972.

[54] U. Niederer. The maximal kinematical invariance group of the free schrodinger equation. *Helv. Phys. Acta*, 45:802, 1972.

[55] T. Mehen. On non-relativistic conformal field theory and trapped atoms: Virial theorems and the state-operator correspondence in three dimensions. *Phys. Rev. A*, 78:013614, 2007.

[56] F. Werner and Y. Castin. The unitary gas in an isotropic harmonic trap: symmetry properties and applications. *Phys. Rev. A*, 74:053604, 2006.

[57] F. Werner and Y. Castin. The unitary three-body problem in a trap. *Phys. Rev. Lett.*, 97:150401, 2006.

[58] D. T. Son. Three comments on the fermi gas at unitarity in a harmonic trap. *ArXiv:0707.1851.*

[59] S. Tan. Energetics of a strongly correlated fermi gas. *Ann. Phys.*, 323:2952, 2008.

[60] S. Tan. Large momentum part of fermions with large scattering length. *Ann. Phys.*, 323:2971, 2008.

[61] S. Tan. Generalized virial theorem and pressure relation fir a strongly correlated fermi gas. *Ann. Phys.*, 323:2987, 2008.
[62] S. Zhang and A. J. Leggett. Sum-rule analysis of radio-frequency spectroscopy of ultracold fermi gas. *Phys. Rev. A*, 77:033614, 2008.
[63] F. Werner. Virial theorems for trapped cold atoms. *Phys. Rev. A*, 78:025601, 2008.
[64] E. Braaten and L. Platter. Exact relations for a strongly-interacting fermi gas from the operator product expansion. *Phys. Rev. Lett.*, 100:205301, 2008.
[65] E. Braaten, D. Kang, and L. Platter. Short-time operator product expansion for rf spectroscopy of a strongly interacting fermi gas. *Phys. Rev. Lett*, 104:223004, 2010.
[66] D. T. Son and E. G. Thompson. Short-distance and short-time structure of a unitary fermi gas. *Phys. Rev. A*, 81:063634, 2010.
[67] M. Randeria E. Taylor. Viscosity of strongly interacting quantum uids: Spectral functions and sum rules. *Phys. Rev. A*, 81:053610, 2010.
[68] E. Braaten. *BCS-BEC crossover and the Unitary Fermi Gas (Lecture Notes in Physics), edited by W. Zwerger.* Springer-Verlag, Berlin, 2011.
[69] G. P. Lepage. What is renormalization? 1989.
[70] G.P. Lepage. How to renormalize the Schrodinger equation. pages 135–180, 1997.
[71] J. W. Negele and H. Orland. *Quantum Many-Particle Systems.* Addison-Wesley, Redwood City, CA, 1988.
[72] J. Zinn-Justin. *Quantum Field Theory and Critical Phenomena 3rd ed.* Clarendon Press, Oxford, 1996.
[73] G. H. Golub and C. F. Van Loan. *Matrix Computations, 3rd Ed.* Johns-Hopkins University Press, Baltimore and London, 1996.
[74] A. Privitera, M. Capone, and C. Castellani. Finite-density corrections to the unitary fermi gas: A lattice perspective from dynamical mean-field theory. *Phys. Rev. B*, 81:014523, 2010.
[75] A. Privitera and M. Capone. Lattice approaches to dilute fermi gases: Legacy of broken galilean invariance. *Phys. Rev. A*, 85:013640, 2012.
[76] F. Werner and Y. Castin. General relations for quantum gases in two and three dimensions. i. two-component fermions. 97, 2006.
[77] D. Lee. Lattice simulations for few- and many-body systems. *Prog. Part. Nucl. Phys.*, 63:117, 2009.
[78] R. Blankenbecler, D. J. Scalapino, and R. L. Sugar. Monte carlo calculations of coupled boson-fermion systems. i. *Phys. Rev. D*, 24:2278, 1981.
[79] R. L. Stratonovich. *Sov. Phys. Dokl.*, 2:416, 1958.
[80] J. Hubbard. *Phys. Rev. Lett.*, 3:77, 1959.
[81] J. E. Hirsch. Discrete hubbard-stratonovich transformation for fermion lattice models. *Phys. Rev. B.*, 28:4059, 1983.
[82] N. Prokof'ev and B. Svistunov. Worm algorithms for classical statistical models. *Phys. Rev. Lett.*, 87:160601, 2001.
[83] O. F. Syljuåsen and A. W. Sandvik. Quantum monte carlo with directed loops. *Phys. Rev. E*, 66:046701, 2002.
[84] D. H. Adams and S. Chandrasekharan. Chiral limit of strongly coupled lattice gauge theories. *Nucl. Phys. B*, 662:220, 2003.
[85] D. Lee. Ground state energy at unitarity. *Phys. Rev. C*, 78:024001, 2008.
[86] M. G. Endres, D. B. Kaplan, J.-W. Lee, and A. N. Nicholson. A new approach for studying large numbers of fermions in the unitary regime. *PoS*, Lattice 2010:182, 2010.
[87] J.-W. Lee, M. G. Endres, D. B. Kaplan, and A. N. Nicholson. Lattice calculation for unitary fermions in a finite box. *PoS*, Lattice 2010:197, 2010.
[88] A. N. Nicholson, M. G. Endres, D. B. Kaplan, and J.-W. Lee. Lattice study of trapped fermions at unitarity. *PoS*, Lattice 2010:206, 2010.
[89] M. G. Endres, D. B. Kaplan, J.-W. Lee, and A. N. Nicholson. Lattice monte carlo calculations for unitary fermions in a finite box. *arXiv:1203.3169*, 2010.
[90] J. Carlson, S. Gandolfi, K. E. Schmidt, and S. Zhang. Auxiliary-field quantum monte carlo method for strongly paired fermions. *Phys. Rev. A*, 84:061602, Dec 2011.
[91] J. E. Drut. Improved lattice operators for non-relativistic fermions. *arXiv:1203.2565, to appear in Phys. Rev. A.*, 2012.
[92] G. Batrouni, A. Hansen, and M. Nelkin. Fourier acceleration of relaxation processes in disordered systems. *Phys. Rev. Lett.*, 57:1336, 1986.
[93] C. Davies, G. Batrouni, G. Katz, A. Kronfeld, P. Lepage, P. Rossi, B. Svetitsky, and K. Wilson. Langevin simulations of lattice field theories using fourier acceleration. *J. Stat. Phys.*, 43:1073, 1986.

[94] C. T. H. Davies, G. G. Batrouni, G. R. Katz, A. S. Kronfeld, G. P. Lepage, K. G. Wilson, P. Rossi, and B. Svetitsky. Fourier acceleration in lattice gauge theories. i. landau gauge fixing. *Phys. Rev. D*, 37:1581, 1988.

[95] G. Katz, G. Batrouni, C. Davies, A. Kronfeld, P. Lepage, P. Rossi, B. Svetitsky, and K. Wilson. Fourier acceleration in lattice gauge theories. ii. matrix inversion and the quark propagator. *Phys. Rev. D*, 37:1589, 1988.

[96] M. Frigo and S. G. Johnson. The design and implementation of fftw3. *Proc. IEEE*, 93:216, 2005.

[97] M. G. Endres, D. B. Kaplan, J.-W. Lee, and A. N. Nicholson. Lattice monte carlo calculations for unitary fermions in a harmonic trap. *Phys. Rev. A*, 84:043644, 2011.

[98] M. Lüscher. Volume dependence of the energy spectrum in massive quantum field theories. 1. stable particle states. *Commun. Math. Phys.*, 104:177, 1986.

[99] M. Lüscher. Volume dependence of the energy spectrum in massive quantum field theories. 2. scattering states. *Commun. Math. Phys.*, 105:153, 1986.

[100] N. Metropolis, A. W. Rosenbluth, M. N. Rosenbluth, A. H. Teller, and E. Teller. Equation of state calculations by fast computing machines. *J. Chem. Phys.*, 21:1087, 1953.

[101] M. Creutz. Monte carlo study of quantized su(2) gauge theory. *Phys. Rev. D*, 21:2308, 1980.

[102] N. Cabibbo and E. Marinari. A new method for updating su(n) matrices in computer simulations of gauge theories. *Phys. Lett. B*, 119:387, 1982.

[103] A. Bazavov, B. A. Berg, and U. M. Heller. Biased metropolis-heat-bath algorithm for fundamental-adjoint su(2). *Phys. Rev. D*, 72:117501, 2005.

[104] R. W. Johnson. General heatbath algorithm for pure lattice gauge theory. *Phys. Rev. D*, 82:114508, 2010.

[105] D. Toussaint. Introduction to algorithms for monte carlo simulations and their application to qcd. *Comput. Phys. Commun.*, 56:69, 1989.

[106] R. H. Swendsen and J. Wang. Nonuniversal critical dynamics in monte carlo simulations. *Phys. Rev. Lett.*, 58:86, 1987.

[107] A. Barbu and S. C. Zhu. Generalizing swendsen-wang to sampling arbitrary posterior probabilities. *IEEE Trans. Patt. Anal. Mach. Intell.*, 27:1239, 2005.

[108] U. Wolff. Collective monte carlo updating for spin systems. *Phys. Rev. Lett.*, 62:361, 1989.

[109] A. Bulgac, J.E. Drut, and P. Magierski. Spin 1/2 fermions in the unitary regime: a superfluid of a new type. *Phys. Rev. Lett.*, 96:090404, 2006.

[110] S. Duane, A. D. Kennedy, B. J. Pendleton, and D. Roweth. Hybrid monte carlo. *Phys. Lett. B*, 195:216, 1987.

[111] S. A. Gottlieb, W. Liu, D. Toussaint, and R. L. Renken. Hybrid-molecular-dynamics algorithms for the numerical simulations of quantum chromodynamics. *Phys. Rev. D*, 35:2531, 1987.

[112] R. Folk I. P. Omelyan, I. M. Mryglod. Symplectic analytically integrable decomposition algorithms: classification, derivation, and application to molecular dynamics, quantum and celestial mechanics simulations. *Comut. Phys. Commun.*, 151:272, 2003.

[113] M. G. Endres, D. B. Kaplan, J.-W. Lee, and A. N. Nicholson. Noise, sign problems, and statistics. *Phys. Rev. Lett.*, 107:201601, 2011.

[114] S. Zhang, J. Carlson, and J. E. Gubernatis. Constrained path quantum monte carlo method for fermion ground states. *Phys. Rev. Lett.*, 74:3652–3655, May 1995.

[115] S. Zhang, J. Carlson, and J. E. Gubernatis. Constrained path monte carlo method for fermion ground states. *Phys. Rev. B*, 55:7464–7477, Mar 1997.

[116] M. Lüscher and U. Wolff. How to calculate the elastic scattering matrix in two-dimensional quantum field theories by numerical simulation. *Nucl.Phys.*, B339:222–252, 1990.

[117] C. Michael. Adjoint sources in lattice gauge theory. *Nuclear Physics B*, 259(1):58 – 76, 1985.

[118] B. Blossier, M. Della Morte, G. von Hippel, T. Mendes, and R. Sommer. On the generalized eigenvalue method for energies and matrix elements in lattice field theory. *JHEP*, 0904:094, 2009.

[119] Z. Fodor and C. Hoelbling. Light Hadron Masses from Lattice QCD. *Rev.Mod.Phys.*, 84:449, 2012.

[120] R. G. Edwards, J. J. Dudek, D. G. Richards, and S. J. Wallace. Excited state baryon spectroscopy from lattice QCD. *Phys.Rev.*, D84:074508, 2011.

[121] J. J. Dudek, R. G. Edwards, M. J. Peardon, D. G. Richards, and C. E. Thomas. Toward the excited meson spectrum of dynamical QCD. *Phys.Rev.*, D82:034508, 2010.

[122] L. Maiani and M. Testa. Final state interactions from Euclidean correlation functions. *Phys.Lett.*, B245:585–590, 1990.

[123] C.J. D. Lin, G. Martinelli, C. T. Sachrajda, and M. Testa. K –¿ pi pi decays in a finite volume. *Nucl.Phys.*, B619:467–498, 2001.

[124] S.R. Beane, P.F. Bedaque, A. Parreno, and M.J. Savage. Two nucleons on a lattice. *Phys.Lett.*, B585:106–114, 2004.
[125] I. Sato and P. F. Bedaque. Fitting two nucleons inside a box: Exponentially suppressed corrections to the Luscher's formula. *Phys.Rev.*, D76:034502, 2007.
[126] P. F. Bedaque, I. Sato, and A. Walker-Loud. Finite volume corrections to pi-pi scattering. *Phys.Rev.*, D73:074501, 2006.
[127] S. R. Beane, W. Detmold, and M. J. Savage. n-Boson Energies at Finite Volume and Three-Boson Interactions. *Phys.Rev.*, D76:074507, 2007.
[128] W. Detmold and M. J. Savage. The Energy of n Identical Bosons in a Finite Volume at O(L**-7). *Phys.Rev.*, D77:057502, 2008.
[129] B. Smigielski and J. Wasem. Ground-state energy shift of n pions and m kaons in a finite volume. *Phys.Rev.*, D79:054506, 2009.
[130] S. R. Beane, W. Detmold, Thomas C. Luu, K. Orginos, M. J. Savage, et al. Multi-Pion Systems in Lattice QCD and the Three-Pion Interaction. *Phys.Rev.Lett.*, 100:082004, 2008.
[131] W. Detmold, M. J. Savage, A. Torok, S. R. Beane, T. C. Luu, et al. Multi-Pion States in Lattice QCD and the Charged-Pion Condensate. *Phys.Rev.*, D78:014507, 2008.
[132] W. Detmold, K. Orginos, M. J. Savage, and A. Walker-Loud. Kaon Condensation with Lattice QCD. *Phys.Rev.*, D78:054514, 2008.
[133] W. Detmold and B. Smigielski. Lattice QCD study of mixed systems of pions and kaons. *Phys.Rev.*, D84:014508, 2011.
[134] W. Detmold, K. Orginos, and Z. Shi. Lattice QCD at non-zero isospin chemical potential. 2012.
[135] X. Li and C. Liu. Two particle states in an asymmetric box. *Phys.Lett.*, B587:100–104, 2004.
[136] X. Feng, X. Li, and C. Liu. Two particle states in an asymmetric box and the elastic scattering phases. *Phys.Rev.*, D70:014505, 2004.
[137] T. Luu and M. J. Savage. Extracting Scattering Phase-Shifts in Higher Partial-Waves from Lattice QCD Calculations. *Phys.Rev.*, D83:114508, 2011.
[138] S. Koenig, D. Lee, and H.-W. Hammer. Volume Dependence of Bound States with Angular Momentum. *Phys.Rev.Lett.*, 107:112001, 2011.
[139] S. Koenig, D. Lee, and H.-W. Hammer. Non-relativistic bound states in a finite volume. *Annals Phys.*, 327:1450–1471, 2012.
[140] K. Rummukainen and S. A. Gottlieb. Resonance scattering phase shifts on a nonrest frame lattice. *Nucl.Phys.*, B450:397–436, 1995.
[141] C.H. Kim, C.T. Sachrajda, and S. R. Sharpe. Finite-volume effects for two-hadron states in moving frames. *Nucl.Phys.*, B727:218–243, 2005.
[142] S. Bour, S. Koenig, D. Lee, H.-W. Hammer, and Ulf-G. Meissner. Topological phases for bound states moving in a finite volume. *Phys.Rev.*, D84:091503, 2011.
[143] Z. Davoudi and M. J. Savage. Improving the Volume Dependence of Two-Body Binding Energies Calculated with Lattice QCD. *Phys.Rev.*, D84:114502, 2011.
[144] R. A. Briceno and Z. Davoudi. Moving Multi-Channel Systems in a Finite Volume. 2012.
[145] M. T. Hansen and S. R. Sharpe. Multiple-channel generalization of Lellouch-Luscher formula. 2012.
[146] B. Borasoy, E. Epelbaum, H. Krebs, D. Lee, and U.-G. Meissner. Two-particle scattering on the lattice: Phase shifts, spin-orbit coupling, and mixing angles. *Eur.Phys.J.*, A34:185–196, 2007.
[147] T. Busch, B.-G. Englert, M. Wilkens, and K. Rza. Two cold atoms in a harmonic trap. *Foundations of Physics*, 28(4):549–559, 1998.
[148] S.-K. Yip. Energy levels of two identical fermions in a harmonic trap near a p-wave feshbach resonance. *Phys. Rev. A*, 78:013612, Jul 2008.
[149] A. Suzuki, Y. Liang, and R. K. Bhaduri. Two-atom energy spectrum in a harmonic trap near a feshbach resonance at higher partial waves. *Phys. Rev. A*, 80:033601, Sep 2009.
[150] W.C. Haxton. The Form of the Effective Interaction in Harmonic-Oscillator-Based Effective Theory. 2007.
[151] W.C. Haxton and T. Luu. Perturbative effective theory in an oscillator basis? *Phys.Rev.Lett.*, 89:182503, 2002.
[152] I. Stetcu, B.R. Barrett, and U. van Kolck. No-core shell model in an effective-field-theory framework. *Phys.Lett.*, B653:358–362, 2007.
[153] T. Luu and A. Schwenk. Three-Fermion Problems in Optical Lattices. *Physical Review Letters*, 98(10):103202, March 2007.
[154] I. Stetcu, B. R. Barrett, U. van Kolck, and J. P. Vary. Effective theory for trapped few-fermion systems. *Phys.Rev.*, A76(6):063613, December 2007.

[155] I. Stetcu, J. Rotureau, B. R. Barrett, and U. van Kolck. Effective interactions for light nuclei: an effective (field theory) approach. *Journal of Physics G Nuclear Physics*, 37(6):064033, June 2010.

[156] U. van Kolck. Nuclear Physics from QCD. *talk given at DOE workshop Forefront Questions in Nuclear Science and the Role of High Performance Computing*, January 2009.

[157] T. Luu, M. J. Savage, A. Schwenk, and J. P. Vary. Nucleon-Nucleon Scattering in a Harmonic Potential. *Phys.Rev.*, C82:034003, 2010.

[158] I. Stetcu, J. Rotureau, B. R. Barrett, and U. van Kolck. An effective field theory approach to two trapped particles. *Annals of Physics*, 325:1644–1666, August 2010.

[159] J. E. Drut, T. A. Lähde, and T. Ten. Momentum distribution and contact of the unitary fermi gas. *Phys. Rev. Lett.*, 106:205302, 2011.

[160] J. E. Drut, T. A. Lähde, G. Wlazłowski, and P. Magierski. The equation of state of the unitary fermi gas: An update on lattice calculations. *Phys. Rev. A*, 85:051601(R), 2011.

[161] G. P. Lepage. The analysis of algorithms for lattice field theory . 1989.

[162] S. R. Beane, W. Detmold, T. C. Luu, K. Orginos, A. Parreno, et al. High Statistics Analysis using Anisotropic Clover Lattices: (I) Single Hadron Correlation Functions. *Phys.Rev.*, D79:114502, 2009.

[163] S. R. Beane, W. Detmold, T. C. Luu, K. Orginos, A. Parreno, et al. High Statistics Analysis using Anisotropic Clover Lattices. II. Three-Baryon Systems. *Phys.Rev.*, D80:074501, 2009.

[164] S. R. Beane et al. High Statistics Analysis using Anisotropic Clover Lattices: (III) Baryon-Baryon Interactions. *Phys.Rev.*, D81:054505, 2010.

[165] M. G. Endres, D. B. Kaplan, J.-W. Lee, and A. N. Nicholson. Listening to Noise. 2011.

[166] A. N. Nicholson. N-body Efimov states from two-particle noise. 2012.

[167] A. C. Berry. The Accuracy of the Gaussian Approximation to the Sum of Independent Variates. *Transactions of the American Mathematical Society*, 49(1):122–136, 1941.

[168] C.-G. Esseen. On the Liapunoff limit of error in the theory of probability. *Arkiv f matematik, astronomi och fysik*, A28:1–19, 1942.

[169] T. DeGrand. Log-normal distribution for correlators in lattice QCD? 2012.

[170] J. Carlson, S.-Y. Chang, V. R. Pandharipande, and K. E. Schmidt. Superfluid fermi gases with large scattering length. *Phys. Rev. Lett.*, 91:050401, 2003.

[171] K. Symanzik in. *Recent Developments in Gauge Theories*. Plenum, New York, 1980. edited by G. 't Hooft *et al*.

[172] K. Symanzik in. *Mathematical Problems in Theoretical Physics*. Springer, New York, 1982. edited by R. Schrader *et al*.

[173] K. Symanzik. Continuum limit and improved action in lattice theories: (i). principles and ϕ^4 theory. *Nuclear Physics B*, 226(1):187 – 204, 1983.

[174] K. Symanzik. Continuum limit and improved action in lattice theories: (ii). o(n) non-linear sigma model in perturbation theory. *Nuclear Physics B*, 226(1):205 – 227, 1983.

[175] S. Tan. Short Range Scaling Laws of Quantum Gases With Contact Interactions. *eprint arXiv:cond-mat/0412764*, December 2004.

[176] D. Blume and K. M. Daily. Trapped two-component Fermi gases with up to six particles: Energetics, structural properties, and molecular condensate fraction. *Comptes Rendus Physique*, 12:86–109, January 2011.

[177] L. Pricoupenko and Y. Castin. Three fermions in a box at the unitary limit: universality in a lattice model. *Journal of Physics A Mathematical General*, 40:12863–12872, October 2007.

[178] H. Bethe and R. Peierls. Quantum Theory of the Diplon. *Proceedings of the Royal Society of London. Series A, Mathematical and Physical Sciences, Volume 148, Issue 863, pp. 146-156*, 148:146–156, January 1935.

[179] S. Bour, H.-W. Hammer, D. Lee, and Ulf-G. Meissner. Benchmark calculations for elastic fermion-dimer scattering. 2012.

[180] G.V. Skornyakov and K.A. Ter-Martirosyan. *Sov. Phys. JETP*, 1957.

[181] D. S. Petrov. Three-body problem in fermi gases with short-range interparticle interaction. *Phys. Rev. A*, 67:010703, Jan 2003.

[182] D. S. Petrov, C. Salomon, and G. V. Shlyapnikov. Scattering properties of weakly bound dimers of fermionic atoms. *Phys.Rev.*, A71:012708, 2005.

[183] S. Bour, X. Li, D. Lee, U.-G. Meissner, and L. Mitas. Precision benchmark calculations for four particles at unitarity. *Phys.Rev.*, A83:063619, 2011.

[184] F. Werner and Y. Castin. Unitary Quantum Three-Body Problem in a Harmonic Trap. *Phys. Rev. Lett.*, 97(15):150401, October 2006.

[185] D. Blume, J. von Stecher, and C. H. Greene. Universal Properties of a Trapped Two-Component Fermi Gas at Unitarity. *Physical Review Letters*, 99(23):233201, December

2007.

[186] S.Y. Chang and G.F. Bertsch. Unitary Fermi gas in a harmonic trap. *Phys.Rev.*, A76:021603, 2007.

[187] K. M. O'Hara, S. L. Hemmer, M. E. Gehm, S. R. Granade, and J. E. Thomas. Observation of a strongly interacting degenerate fermi gas of atoms. *Science*, 298:2179, 2002.

[188] J. R. Engelbrecht, M. Randeria, and C. A. R. Sá de Melo. Bcs to bose crossover: Broken-symmetry state. *Phys. Rev. B*, 55:15153–15156, Jun 1997.

[189] M. E. Gehm, S. L. Hemmer, S. R. Granade, K. M. O'Hara, and J. E. Thomas. Mechanical stability of a strongly interacting Fermi gas of atoms. *Phys. Rev. A*, 68, 2003.

[190] S. Y. Chang, V. R. Pandharipande, J. Carlson, and K. E. Schmidt. Quantum monte carlo studies of superfluid fermi gases. *Phys. Rev. A*, 70:043602, 2004.

[191] G. A. Baker. Neutron matter model. *Phys. Rev. C*, 60:054311, Oct 1999.

[192] T. Bourdel, L. Khaykovich, J. Cubizolles, J. Zhang, F. Chevy, M. Teichmann, L. Tarruell, S. J. J. M. F. Kokkelmans, and C. Salomon. Experimental study of the bec-bcs crossover region in lithium 6. *Phys. Rev. Lett.*, 93:050401, Jul 2004.

[193] G. E. Astrakharchik, J. Boronat, J. Casulleras, and S. Giorgini. Equation of state of a fermi gas in the bec-bcs crossover: A quantum monte carlo study. *Phys. Rev. Lett.*, 93:200404, Nov 2004.

[194] M. Bartenstein, A. Altmeyer, S. Riedl, S. Jochim, C. Chin, J. Hecker Denschlag, and R. Grimm. Crossover from a molecular Bose-Einstein condensate to a degenerate Fermi gas. *Phys. Rev. Lett.*, 92:120401, 2004.

[195] J. Carlson and Sanjay Reddy. Asymmetric two-component fermion systems in strong coupling. *Phys. Rev. Lett.*, 95:060401, Aug 2005.

[196] J. V. Steele. Effective Field Theory Power Counting at Finite Density. *ArXiv Nuclear Theory e-prints*, October 2000.

[197] J. Kinast, A. Turlapov, J.E. Thomas, Q. Chen, J. Stajic, and K. Levin. Heat capacity of a strongly interacting Fermi gas. *Science*, 307:1296, 2005.

[198] D. Lee and T. Schäfer. Cold dilute neutron matter on the lattice. ii. results in the unitary limit. *Phys. Rev. C*, 73:015202, Jan 2006.

[199] H. Heiselberg. Fermi systems with long scattering lengths. *Phys. Rev. A*, 63:043606, 2001.

[200] G. B. Partridge, W. Li, R. I. Kamar, Y. Liao, and R. G. Hulet. Pairing and phase separation in a polarized Fermi gas. *Science*, 311:503, 2006.

[201] A. Bulgac, J. E. Drut, and P. Magierski. Spin 1/2 fermions in the unitary regime: A superfluid of a new type. *Phys. Rev. Lett.*, 96:090404, Mar 2006.

[202] A. Perali, P. Pieri, and G. C. Strinati. Quantitative comparison between theoretical predictions and experimental results for the bcs-bec crossover. *Phys. Rev. Lett.*, 93:100404, Sep 2004.

[203] C. A. Regal, M. Greiner, S. Giorgini, M. Holland, and D. S. Jin. Momentum distribution of a fermi gas of atoms in the bcs-bec crossover. *Phys. Rev. Lett.*, 95:250404, Dec 2005.

[204] D. Lee. Ground-state energy of spin-$\frac{1}{2}$ fermions in the unitary limit. *Phys. Rev. B*, 73:115112, Mar 2006.

[205] T. Schäfer, C.-W. Kao, and S. R. Cotanch. Many body methods and effective field theory. *Nuclear Physics A*, 762:82–101, November 2005.

[206] J. T. Stewart, J. P. Gaebler, C. A. Regal, and D. S. Jin. Potential energy of a ^{40}K fermi gas in the bcs-bec crossover. *Phys. Rev. Lett.*, 97:220406, Nov 2006.

[207] O. Juillet. Sign-free stochastic mean-field approach to strongly correlated phases of ultracold fermions. *New Journal of Physics*, 9(6):163, 2007.

[208] L. Luo and J. Thomas. Thermodynamic measurements inastrongly interacting fermigas. *Journal of Low Temperature Physics*, 154:1–29, 2009. 10.1007/s10909-008-9850-2.

[209] D. Lee. The symmetric heavy-light ansatz. *The European Physical Journal A - Hadrons and Nuclei*, 35:171–187, 2008. 10.1140/epja/i2008-10537-2.

[210] N. Navon, S. Nascimbène, F. Chevy, and C. Salomon. The equation of state of a low-temperature fermi gas with tunable interactions. *Science*, 328(5979):729–732, 2010.

[211] T. Papenbrock. Density-functional theory for fermions in the unitary regime. *Phys. Rev. A*, 72:041603, Oct 2005.

[212] S. Nascimbène, N. Navon, K. J. Jiang, F. Chevy, and C. Salomon. Exploring the thermodynamics of a universal Fermi gas. *Nature*, 463:1057–1060, February 2010.

[213] Y. Nishida and D. T. Son. expansion for a fermi gas at infinite scattering length. *Phys. Rev. Lett.*, 97:050403, Aug 2006.

[214] M. J. H. Ku, A. T. Sommer, L. W. Cheuk, and M. W. Zwierlein. Revealing the superfluid lambda transition in the universal thermodynamics of a unitary fermi gas. *Science*, 2012.

[215] R. Haussmann, W. Rantner, S. Cerrito, and W. Zwerger. Thermodynamics of the bcs-bec

crossover. *Phys. Rev. A*, 75:023610, Feb 2007.

[216] M. Y. Veillette, D. E. Sheehy, and L. Radzihovsky. Large-n expansion for unitary superfluid fermi gases. *Phys. Rev. A*, 75:043614, Apr 2007.

[217] T. Abe and R. Seki. From low-density neutron matter to the unitary limit. *Phys. Rev. C*, 79:054003, May 2009.

[218] P. Arnold, J. E. Drut, and D. T. Son. NNLO epsilon expansion for a Fermi gas at infinite scattering length. *Phys. Rev. A*, 75:043605, 2006.

[219] P. Magierski, G. Wlazłowski, A. Bulgac, and J. E. Drut. Finite-temperature pairing gap of a unitary fermi gas by quantum monte carlo calculations. *Phys. Rev. Lett.*, 103:210403, Nov 2009.

[220] S. Gandolfi, K. E. Schmidt, and J. Carlson. Bec-bcs crossover and universal relations in unitary fermi gases. *Phys. Rev. A*, 83:041601(R), 2011.

[221] M. M. Forbes, S. Gandolfi, and A. Gezerlis. Resonantly interacting fermions in a box. *Phys. Rev. Lett.*, 106:235303, Jun 2011.

[222] X. Li, J. Kolorenč, and L. Mitas. Atomic fermi gas in the unitary limit by quantum monte carlo methods: Effects of the interaction range. *Phys. Rev. A*, 84:023615, Aug 2011.

[223] Y. Nishida and D. T. Son. Fermi gas near unitarity around four and two spatial dimensions. *Phys. Rev. A*, 75:063617, Jun 2007.

[224] Chen Ji-Sheng. Ground state energy of unitary fermion gas with the thomson problem approach. *Chinese Physics Letters*, 24(7):1825, 2007.

[225] Y. Nishida. Ground-state energy of the unitary fermi gas from the expansion. *Phys. Rev. A*, 79:013627, Jan 2009.

[226] M. Tinkham. *Group Theory and Quantum Mechanics*. Dover Publications, Inc., Mineola, New York, 1992.